Edition : 01
Volume : 01

E-ISSN : 2800-1729

Biopolymer Applications Journal

Editor in chief:
Dr. HAMMICHE Dalila

UNIVERSITÉ ABDERRAHMANE MIRA - BEJAIA
FACULTÉ DE TECHNOLOGIE

Biopolymer Applications Journal

Editorial

Biopolymer Applications Journal is a specialized scientific journal, created in 2021 and published by the ***Faculty of Technology, University of Bejaia***. It appears twice a year and fills the need for researchers and engineering in biopolymers field. The journal is a space for inspiring ideas and discussions of advances in the field of biopolymer applications in a wide range of disciplines for the publication of high-quality peer-reviewed original papers and review articles.

The journal is interdisciplinary in regard to contributions and covers the following subjects:

-Ageing; Biochemistry; Bioengineering; biomaterials, biomedical engineering; mechanical engineering; modeling and simulation; polymers and plastics and other related topics.

Journal Information

Biopolymer Applications Journal is a new Journal, where we aim to work towards spreading awareness about various disciplines amongst people from all walks of life through publication of articles with this Journal. We are offering you open Access, Peer-Reviewed, Rapid, and free Publication

e-ISSN 2800-1729
Site web: http://www.univ-bejaia.dz/baj/
Contact: baj.contact@yahoo.com
online submission: http://univ-bejaia.dz/revueBaj

Editor-in-Chief
Dr. Dalila HAMMICHE
Université de Bejaia, Algeria
Baj.contact@yahoo.com
Dalila.hammiche@univ-bejaia.dz

Table of content

Stability ring lactone study of camptothecin and irinotecan in artificial media and Human plasma

Sofiane FATMI[*1, 2, 3], Lamia TAOUZINET [1, 2], Zahra TOUTOU [1, 4], Nacera CHIBANI [4] Mohamed SKIBA [3] and Mokrane IGUER-OUADA [2]

[1] *Department of Processes Engineering, Faculty of Technology, Technology Pharmaceutical Laboratory, Université de Bejaia, 06000, Bejaia, Algeria.*

[2] *Faculty of Nature and Life Sciences, Associated Laboratory in Marine Ecosystems and Aquaculture, Université de Bejaia, 06000, Bejaia, Algeria.*

[3] *Technology Pharmaceutical and Bio pharmaceutics Laboratory, UFR Medicine and Pharmacy, Rouen University, 22 Blvd. Gambetta, 76183, Rouen, France.*

[4]*LMPA, Department of Process Engineering, Faculty of Technology, Université de Bejaia, Bejaia 06000, Algeria*

*Corresponding author** sofiane.fatmi@univ-bejaia.dz

Received: 01 January 2022; Accepted: 24 January 2022; Published: 27 January 2022

Abstract

Camptothecin is a promising anti-colorectal cancer agent. However, its use in clinical medicine is compromised by its low solubility and high instability in physiological media. The present work aims to study the chemical stability of the camptothecin lactone ring (alone, encapsulated, and in solid dispersion) while comparing it to that of a reference analog irinotecan. This stability is studied in acidic (pH 2) and physiological (saline) media and Human plasma by high performance liquid chromatography (HPLC). Stability tests carried out on CPT alone, encapsulated and in solid dispersion in artificial media and Human plasma demonstrate that ternary systems [CPT/β-CDs/PEG 6000 and CPT/PM-βCDs/PEG 6000] can lead to the protection of CPT lactone ring in physiological media and Human plasma for 72 hours. This protection is essential to the camptothecin therapeutic effect when administered in pharmaceutical form.

Keywords: *Camptothecin, Chemical Stability, Colorectal Cancer, Cyclodextrin, Irinotecan, Polyethylene Glycol, Solid Dispersion.*

I. Introduction

One of the most promising anti-colorectal cancer agents is camptothecin (CPT, Figure 1), which is a pentacyclic alkaloid with a pyrroloquinoline motif [1]. This pale-yellow crystalline powder is extracted from an Asian tree called Camptotheca Acuminata. Camptothecin is a non-competitive inhibitor of topoisomerase I, as it binds neither to the enzyme itself nor to DNA but binds to both at the same time (DNA-Topoisomerase I) to form a reversible ternary complex (DNA-Topoisomerase I-Camptothecin) called cleavable complex which will inhibit the action of the enzyme by irreversibly cutting DNA in multiple locations, leading to cell death. Despite its remarkable anticancer activity, camptothecin is insoluble in water and physiological media, its dissolution is obtained in dimethyl sulfoxide (DMSO). Moreover, it is unstable in physiological media due to the hydrolysis of its lactone ring leading to the loss of its biological activity [2].

Thus, despite the proven therapeutic potential of camptothecin (CPT), it has not been exploited in therapy. However, it has been the source of a more soluble and less unstable analog such as irinotecan (CPT 11, Figure 1) [3].

However, other solutions have been studied by researchers such as encapsulation by cyclodextrins, nanofibrous silica microparticles, liposomes, and solid dispersion in polyethylene glycol (PEG) [4-7]. In addition, numerous research has been carried out to overcome the lack of solubility and stability of camptothecin in physiological media, using encapsulation with cyclodextrins (CDs), solid dispersion in polyethylene glycol (PEG), and/or the formation of ternary systems (CPT-CD-PEG) [4].

Cyclodextrins (CDs) are cyclic oligosaccharides composed of 6 to 12 glucopyranosyl subunits linked by -(1,4) glycosidic bonds. The CDs containing more than 8 glucopyranosyl units are not stable enough for pharmaceutical use. The most common CDs are the native ones (cyclodextrins no branching other than the glycosidic , and 8 glucopyranose residues respectively, all having the chair configuration. The CD is characterized by a "crown" structure and is in the form of a truncated cone ring with primary and secondary hydroxyls on the outside and hydrogen, carbon and ether-oxide bonds on the inside, their structures are given in Figure 2 [8].

To improve the properties of cyclodextrins, numerous derivatives have been developed: Hydroxypropyl-beta-CD (HP- -CD), Per methyl-beta-CD (PM- -CD), Sulfobuthyl-beta-CD (SBE- -CD), Hydroxypropyl-gamma-CD (HP- -CD). The chemical modifications concern the hydroxyl groups, which are substituted in varying numbers depending on the type of native cyclodextrin [9].

Because of the truncated cone structure and the particular position of the hydroxyls, cyclodextrins are amphiphilic and therefore have two distinct zones of polarity. The outside of the cavity and the ends are polar. Thus, it is the primary and secondary hydroxyls on the edges of the cone that make this molecule soluble in water. On the other hand, the inner of the cavity where oxygens are found is less polar. This more hydrophobic area will play an important function in the inclusion of the hydrophobic host molecules.

Indeed, FATMI et al. [4,5] have established that camptothecin encapsulated by cyclodextrins becomes more soluble especially when using methyl-beta-CD, indicating a potential increased bioavailability.

Also, it is now known that solid dispersion (SD) increases the solubility of drugs converting them into amorphous crystals, by reducing their particle size and by increasing their wettability [10]. In this process polyethylene glycols (PEGs, Figure 2) are very often used as water-soluble polymeric matrix [10], they are non-toxic and biocompatible. The Food and Drug Administration (FDA) has approved their use in intravenous, oral, and dermal pharmaceutical preparations [11].

A. Paudel et al. [12] have demonstrated that it is possible to improve the solubility of hydrophobic molecules in general and naproxen in particular through solid dispersion. X. Wang et al also used solid dispersion in PEG and Polyvinyl pyrrolidone (PVP) to improve the solubility of two highly lipid soluble molecules, namely, itraconazole and indomethacin, resulting in binary (PA/polymer) and ternary systems [(PA/surfactant)/polymer] with very satisfactory dissolution percentages [13].

The present work aims to study the chemical stability (lactone ring) that guarantees the anticancer activity of camptothecin (alone, encapsulated and in solid dispersion) while comparing it to that of a reference analog CPT 11. This stability is studied in acidic, physiological, and human plasma by high-performance liquid chromatography (HPLC).

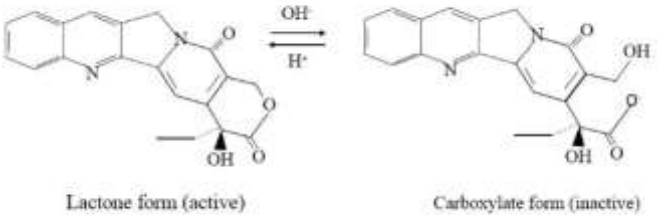

Figure 1: Camptothecin and irinotecan structure.

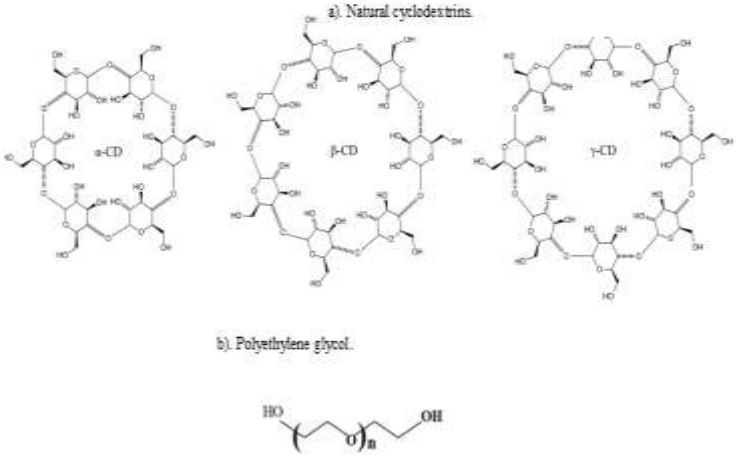

Figure 2: Chemical structures a) Natural cyclodextrins. b) Polyethylene glycol.

II. Material and methods

II.1. Materials

- Camptothecin (M_w 348.11 g/mol) and irinotecan (M_w 586.678 g/mol) were purchased from Shenzhen Boda Natural Product laboratory (P. R. China).
- Cyclodex - -CDs were obtained from Roquette Fréres (France).
- Polyethylene glycol 6000 was obtained from BASF (Germany).
- All reagents were of analytical grade.

II.2. Methods

Complexes and solid dispersion preparations

- Binary system (CPT/CDs inclusion complexes and CPT/PEG 6000) preparation

Cyclodextrins and CPT (1:1 molar ratio) were dissolved in 50 ml of ethanol, the mixture was left under agitation for 1 hour protected from light. After drying at 45°C for 1 hour, the powder was preserved in a desiccator [4].

- Ternary system (Solid dispersion of CPT complexes in PEG 6000) preparation

Nine parts of polyethylene glycol 6000 and one part of the CPT complexed form were dissolved in 50 ml ethanol by agitation. After drying at 45°C for 1 hour, the powder was preserved in a desiccator [4].

Study of CPT (free, encapsulated, or solid dispersion) and CPT 11 lactone ring stability in artificial media pH 2 and physiological serum

Five mg of camptothecin (free, encapsulated, or solid dispersion) and irinotecan were shaken for 72 hours in the dark in 500 ml of pH 2 buffer media and physiological media (saline). At appropriate time (1 H and 72 H), the solutions were filtered and quantified by HPLC. The analyses were carried out in triplicate.

Study of CPT (free, encapsulated, or solid dispersion) and CPT 11 lactone ring stability in human plasma

Investigations were performed with new blood. The blood was centrifuged at 6000 for 15 min at room temperature to isolate plasma and buffy coats. The plasma was supplanted by an isotonic arrangement (NaCl 0.9%). Then, plasma was treated with various arrangements at 0.01 mg/ml (v/v) (CPT, CPT11 and CPT binary and ternary systems). The samples were shaken for 72 hours in the dark. At the appropriate time (1 H and 72 H), the solutions were filtered and quantified by HPLC. The analyses were carried out in triplicate.

HPLC analyses

The analysis of lactone and carboxylate forms of CPT and CPT 11, were performed using HPLC-UV system (UltiMate 3000 RS-Variable Wavelength detector) which consisted of an auto-injector LC 1650, consisting of vacuum degasser, temperature-controlled well-plate autosampler, column thermostat, quaternary pump, and photodiode array detector set at 365 nm. Chromatographic analysis was performed using a Hypersil ODS C-18 (150 x 4.6 mm, 5 µm particle

USA). The mobile phase consisted of a mixture of a borate buffer and acetonitrile (65: 35, v/v) with a flow rate of 1 ml/min, at a temperature of 30 °C and with an injection volume of 20 µl. Standard solutions were prepared by dissolving CPT or CPT 11 in a mixture of methanol/DMSO (95:5, v/v).

III. Results and discussion

Study of CPT and CPT 11 lactone ring stability in artificial media pH 2, physiological serum, and Human plasma

Chromatograms resulting from HPLC analysis of the lactone and carboxylate forms of CPT alone and CPT 11 solubilized in various media are shown in Figure 3.

The first stage of this work was to investigate the behavior of CPT and CPT 11 in various media: pH 2, saline and human plasma as a function of time (1 H and 72 H). Figure 4 summarizes the resulting data.

The findings show that camptothecin is stable in pH 2 media even after 72 H in solution. On the other hand, it is clear that in saline and human plasma, from the first hour, CPT is denatured and transformed into the inactive carboxylated form. Indeed, it is known that the lactone cycle of camptothecin is pH-dependent [14]. It was also observed that the CPT derivative (CPT 11) is stable regardless of the media and time of analysis, showing a small degradation.

The results are justified by those of FATMI et al. [4,5] for the encapsulation or/and solid dispersion of CPT not only to solubilize it but also to protect it during human administration.

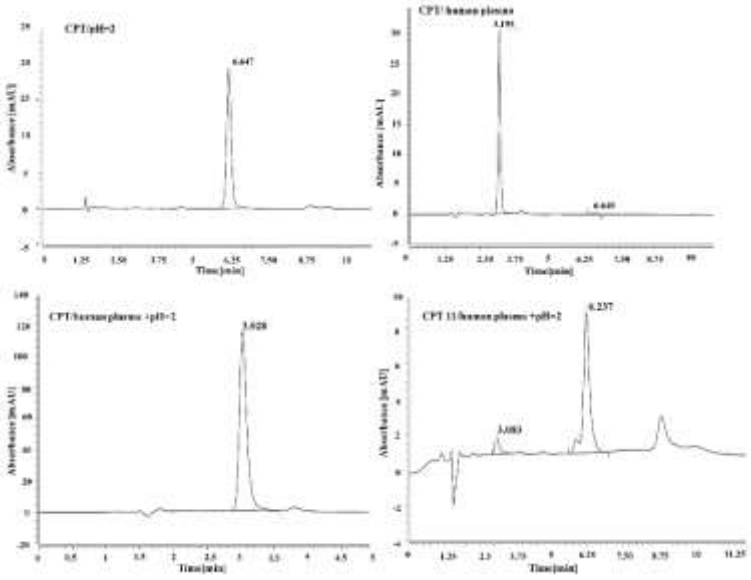

Figure 3: HPLC Chromatograms of the lactone and carboxylate forms of CPT alone and CPT 11 solubilized in various media

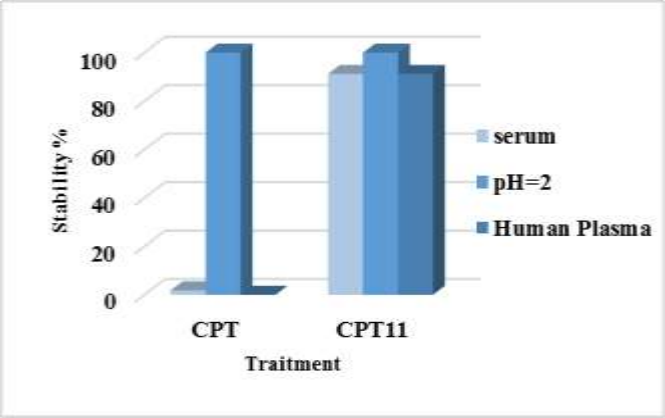

Figure 4: Stability of CPT and CPT 11 in the media: pH 2, serum and human plasma.

Study of CPT (alone, encapsulated or/and dispersed) and CPT 11 lactone ring stability in artificial media pH 2, physiological serum and Human plasma

Chromatograms resulting from HPLC analysis of the lactone and carboxylate forms of CPT (alone, encapsulated and in solid dispersion) and CPT 11 solubilized in various media are shown in Figure 5.

The results of the investigation of the behavior of CPT (alone, encapsulated or/and dispersed) and CPT 11 in various media: pH 2, saline and human plasma as a function of time (1 H and 72 H) are summarized in Figure 6.

All preparations were showing that camptothecin (alone, encapsulated or/and dispersed) is stable in pH 2 media even after 72 H in solution.

Unlike camptothecin alone, CPT in binary [CPT- -CDs and CPT-PM- , and ternary [-CDs/PEG 6000 and CPT/PM- wed protection from lactone ring degradation. This protection is maximal in CPT

PM-
(irinotecan). It is probably due to the cavity stabilizing effect of CDs. J. Kang et al [15] in their research, had also established this protective capacity.

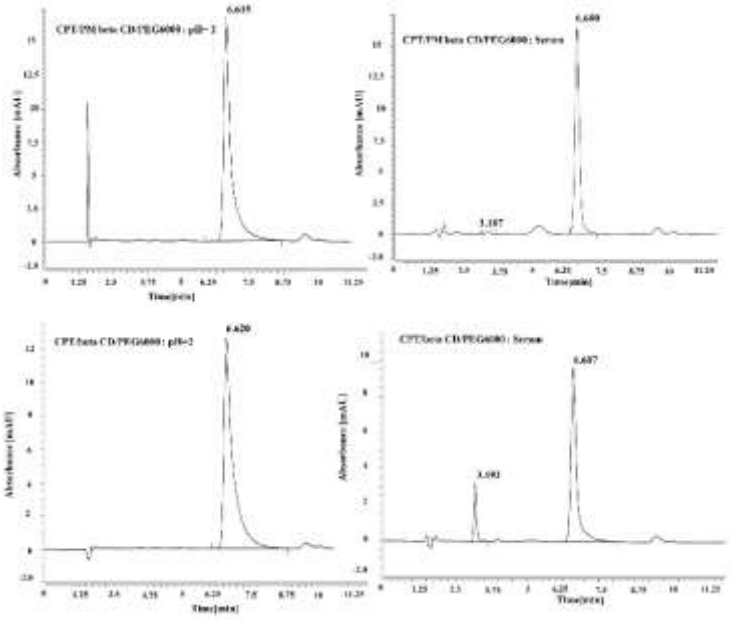

Figure 5: HPLC Chromatograms of the lactone and carboxylate forms of CPT (encapsulated and in solid dispersion) and CPT 11 solubilized in various media.

Among the binary systems, the PM- -based system offers the best protection. This can be attributed to very polar methyl groups, which not only disrupt the intramolecular hydrogen bonding, making the PM-
soluble and stable but also extends the molecule cavity [15].

Also, ternary systems based on both types of CDs offer better percentages of protection (at an equal rate), this is probably due to the presence of PEG 6000 which is a very hydrophilic polymer and is currently widely used as a pharmaceutical carrier for the transport of poorly soluble and stable drugs. But also, it seems that this polymer cancels the effect of the external groups of the cyclodextrin cavity as reported by R. Sawant et al. [16].

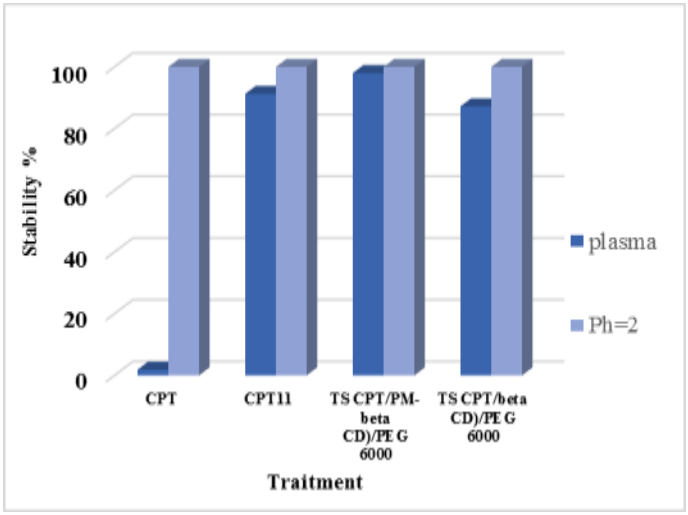

Figure 6: CPT (alone, encapsulated or/and dispersed) and CPT 11 in the media: pH 2, serum and human plasma.

Finally, the stability tests carried out on CPT alone, encapsulated and in solid dispersion in artificial media and human plasma demonstrate that the systems prepared by FATMI et al. [4,5] can lead to the protection of CPT lactone ring, essential to its therapeutic effect when administered in pharmaceutical form.

IV. Conclusions

To ensure the therapeutic effect of camptothecin, it is known that the integrity of the lactone cycle must be assured. Thus, the present work aims to study the chemical stability (lactone ring) of camptothecin (alone, encapsulated and in solid dispersion) while comparing it to that of a reference analog CPT 11. This stability is studied in pH 2, and physiological media and human plasma by high performance liquid chromatography (HPLC). Stability tests carried out on CPT alone, encapsulated and in solid dispersion in artificial media and Human plasma demonstrate that the systems particularly ternary systems [-CDs/PEG 6000 and CPT/PM- EG 6000], can lead to the protection of CPT lactone ring in physiological media, and Human plasma for 72 hours. This protection is essential to the camptothecin therapeutic effect when administered in pharmaceutical form.

Acknowledgment*:*

Ecosystems and Aquaculture, Faculty of Nature and Life

Bio pharmaceutics Laboratory, UFR Medicine and Pharmacy, Rouen Univers
And Direction Générale de la Recherche Scientifique et Développement Technologique, Algeria.

Conflict of interest. The authors report no conflict of interest.

References

[1] L. Qi, Y. Zhang, W. Zhang, Y. Wang, Y. Han, Y. Ding. The inhibition of colorectal cancer growth by the natural product macrocarpal I, Free Radical Biology and Medicine. 16, 2383-391, 2021. https://doi.org/10.1016/j.freeradbiomed.2020.10.317.

[2] M. Ghanbari-Movahed, T. Kaceli, A. Mondal, M.H. Farzaei, A. Bishayee. Recent advances in improved anticancer efficacies of camptothecin nano-formulations: A Systematic Review, Biomedicines. 9, 480, 2021. https://doi.org/10.3390/biomedicines9050480.

[3] Q. Huang, X. Liu, H. Wang, X. Liu, Q. Zhang, K. Li, Y. Chen, Q. Zhu, Y. Shen, M. Sui. A nanotherapeutic strategy to overcome chemoresistance to irinotecan/7-ethyl-10-hydroxy-camptothecin in colorectal cancer, Acta Biomaterialia. 137, 262-275, 2022. https://doi.org/10.1016/j.actbio.2021.10.034.

[4] S. Fatmi, L. Bournine, M. Iguer-Ouada, M. Lahiani, F. Bouchal, M. Skiba. Amorphous solid dispersion studies of camptothecinñcyclodextrin inclusion complexes in PEG 6000. Acta Poloniae Pharmaceutica, 72(1), 179-92, 2015.

[5] S. Fatmi, L. Taouzinet, M. Lahiani-Skiba, M. Skiba, M. Iguer-Ouada. New formulation and evaluation of camptothecin encapsulated and/or dispersed suppository. Anti-Cancer Agents in Medicinal Chemistry. 21, 1183-1190, 2021. https://doi.org/10.2174/1871520620666200903150635.

[6] S. Saraf, A. Jain, A. Tiwari, A. Verma, S.K. Jain. Engineered liposomes bearing camptothecin analogue for tumour targeting: in vitro and ex-vivo studies. Journal of Liposome Research. 1(31), 326-341, 2020. https://doi.org/10.1080/08982104.2020.1801725.

[7] C.-S. Wu, D.-Y. Wu, S.-S. Wang. Heat-regulating polylactic acid/silica aerogel composite fabric: Preparation and characterization. Express Polymer Letter 16, 21-33, 2022. https://doi.org/10.3144/expresspolymlett.2022.3.

[8] A. Dodero, G. Schlatter, A. H´ebraud, S. Vicini, M. Castellano. Polymer-free cyclodextrin and natural polymer-cyclodextrin electrospun nanofibers: A comprehensive review on current applications and future perspectives. Carbohydrate Polymers 264, 118042, 2021. doi: 10.1016/j.carbpol.2021.118042.

[9] M. Petitjean, I.X. García-Zubiri, J.R. Isasi. History of cyclodextrin-based polymers in food and pharmacy: a review. Environmental Chemistry Letters 19, 3465-3476, 2021. https://doi.org/10.1007/s10311-021-01244-5.

[10] S. Alshehri, S.S. Imam, A. Hussain, M.A. Altamimi, N.K. Alruwaili, F. Alotaibi, A. Alanazi, F. Shakeel. Potential of solid dispersions to enhance solubility, bioavailability, and therapeutic efficacy of poorly water-soluble drugs: newer formulation techniques, current marketed scenario and patents. Drug Delivery 27, 1625-1643, 2020. https://doi.org/10.1080/10717544.2020.1846638.

[11] CFR - Code of Federal Regulations Title 21 Polyethylene glycol, Food and Drugs, Food and Drug Administration, indirect food additives: adjuvants, production aids, and sanitizers subpart d - certain adjuvants and production aids. https://www.accessdata.fda.gov

[12] A. Paudel, Z.A. Worku, J. Meeus, S. Guns, G. V. d. Mooter, Manufacturing of solid dispersions of poorly water-soluble drugs by spray drying: Formulation and process considerations. International Journal of Pharmaceutics 453(1), 253-284, 2012. DOI: 10.1016/j.ijpharm.2012.07.015

[13] X. Wang. Physico-chemical characterization of binary and ternary solid dispersions of itraconazole and indomethacin, Phd thesis, 2007.

[14] M.L. Bondì, R. Di Gesù, E.F. Craparo, Lipid Nanoparticles for Drug Targeting to the Brain, in: Methods in Enzymology, Elsevier, pp. 229-251, 2012. https://doi.org/10.1016/B978-0-12-391860-4.00012-4.

[15] J. Kang, V. Kumar, D. Yang, P.R. Chowdhury, R.J. Hohl. Cyclodextrin complexation: influence on the solubility, stability, and cytotoxicity of camptothecin, an antineoplastic agent. European Journal of Pharmaceutical Sciences 15, 163-170, 2002. https://doi.org/10.1016/S0928-0987,0100214-7.

[16] R. Sawant, R. Sawant, V. Torchilin. Mixed PEG PE/vitamin E tumor-targeted immunomicelles as carriers for poorly soluble anti-cancer drugs: Improved drug solubilization and enhanced in vitro cytotoxicity. European Journal of Pharmaceutics and Biopharmaceutics 70, 51-57, 2008. https://doi.org/10.1016/j.ejpb.2008.04.016.

Hydrolytic aging of a biopolymer reinforced with Alfa fiber treated with dispersing agent

Lisa Klaai[1,*], Dalila Hammiche[1], Hanane Ibrahim[1], Amar Boukerrou[1]

[1]*Laboratoire des Matériaux Polymères Avancés (LMPA), Faculté de Technologie, Université de Bejaia, 06000 Bejaia, Algérie*

*Corresponding author** lisa.klaai@univ-bejaia.dz

Received: 01 January 2022; Accepted: 23 January 2022; Published: 27 January 2022

Abstract

The aging of materials is a degradation or a slow evolution of the properties of the material resulting from its intrinsic instability or caused by more or less aggressive external factors. Based on the literature, the degradation of polylactic acid (PLA) biocomposites mainly consists of hydrothermal degradation and photodegradation, the PLA/natural fibers interface is one of the main factors affecting the rate of hydrolytic degradation. With the addition of vegetable fibers, greater degradation is observed. Thus, because of their hydrophobicity, the biocomposite obtained has a greater moisture uptake causing swelling at the fiber/matrix interface. This causes cracking and degradation by more significant chain cuts. This work reports on the hydrolytic aging of biocomposites which were composed of Alfa fiber and Polylactic acid (PLA) prepared by extrusion. To improve the fiber/matrix compatibility, the Alfa fiber has been treated with a dispersing agent which is BYK W-980. Spectroscopic (FTIR), thermal, and water absorption tests before and after hydrolytic aging of biocomposites have been studied and compared. The results revealed that PLA/Alfa biocomposites in the presence of BYK W-980 are more resistant to hydrolytic aging compared to untreated composites.

Keywords: *Alfa Fiber, Biopolymer, Dispersing Agent, Hydrolytic Aging.*

I. Introduction

Chemical aging by hydrolysis (or hydrolytic) is characterized by the degradation of the polymer in an aqueous medium (liquid or gaseous). This type of degradation mainly affects polycondensates such as polyesters and polyamides and in particular PLA which is aliphatic polyester. Hydrolysis is generally characterized by a process of random chain cuts and is controlled by the diffusion of water within the polymer and is catalyzed in the presence of acid or base [1].

As in the case of other types of degradation, hydrolysis tends to act in amorphous zones, which are more permeable to water molecules [2].

In the case of PLA, the hydrolysis of the macromolecular chains produces lactic acid, which makes the reaction auto-catalytic leading to rapid and catastrophic degradation for the material [3]

The hydrolysis mechanism of polyesters induces chain breaks and shows that the species formed are of alcohol and acid type. Due to the formation of shorter chains, Chemi-crystallization takes place, stiffening and weakening the PLA [4].

In addition, low molecular weight oligomers and monomers are formed and leave the parent chains, causing surface erosion with the mass loss [2].

The hydrolysis of PLA has been the subject of numerous studies and has been established as the cause of strong chain breaks, a strong crystallinity of the polymer and therefore a drop in mechanical properties. Badia et al. [5] demonstrated a lower diffusion of water in a material retransformed three times thanks to its highly crystalline character.

The vulnerability of a biocomposite to hydrolytic aging is mainly linked to the fiber/matrix interface which is a very fragile zone. Indeed, aging by water immersion of PP/flax composites was carried out by Arbelaiz et al. [6] to study the kinetics of mass gain by the latter this immersion then caused swelling of the cellulose. This generated shear stresses at the matrix/fiber interface, and therefore their decohesion affected the mechanical properties (modulus and tensile strength) of the biocomposites after immersion [7].

In addition, the temperature can facilitate the diffusion of water molecules within the material.

For example, Joseph et al. [8] observed faster water uptake of PP/sisal composites once the water was heated to 70°C to limit the absorption of water in a humid environment by composites reinforced with natural fibers, the method commonly used consists in increasing the hydrophobicity of the fibers and improving the interfacial adhesion by treating the fibers. For example, the addition of a coupling agent made it possible to limit the water uptake of the biocomposites [9-11].

This present work is focused on the study of the durability of different PLA/Alfa biocomposite

materials treated with BYK W-980 and untreated, prepared via hydrolytic aging.

II. Material and methods

The polymer used in this work is Poly (lactic acid) (2003D grade) in the form of pellets. It was obtained from Nature Works LLC, USA. Alfa used as reinforcement was collected from the arid region of Algeria. The average particles size is <80 µm, obtained using a universal laboratory grinder for plastics and wood "VERDER". The chemical composition of Alfa was reported previously [12].

The dispersing agents have been kindly given by BYK-CHEMIE its properties and Alfa fiber treatment is determined according to Ibrahim et al., [13].

The hydrolytic aging was carried out according to the standard ASTM D570. The specimens (m_0) are immersed in distilled water at 23 °C, with magnetic stirring. Every 24 hours, we take a sample; we remove all the surface water with absorbent paper.

The samples are reweighed (m), the operation continues for 6 months. The variation in mass (Δm) in (%) is given by the following formula:

$$\Delta m(\%) = \frac{m - m_0}{m_0} \times 100$$

Where: Δm (%) is the change in mass (wt. %), m_o is the mass of the sample before immersion (g) and m represents the mass of the sample after immersion (g).

III. Characterization

III.1 Fourier-Transform Infrared Spectroscopy (FTIR)

The samples were dried at 80 °C for one hour and used for infrared spectroscopy analysis. Infrared measurements were made on an FTIR spectrophotometer (SHIMADZU FTIR-8400S). A resolution of 4 cm-1 was used in the 4000-400 cm^{-1} wavenumber region.

III.2 Thermo-Gravimetric Analysis (TGA)

The thermal analysis of biocomposites was realized using a TA instrument Q500. The samples were heated from 20 °C to 800 °C with a heating rate of 10 °C/min under a nitrogen atmosphere with a flowing rate of 50 ml/min.

III.3 Water absorption test

Squares 2 cm wide were dried for 1 hour in an oven at 60 °C and weighed the initial mass (m_0) using a precision analytical balance of 0.0001g, before immersion in distilled water at room temperature. Then, they were removed from the water, gradually, wiped carefully with paper, and then the mass of the samples was weighed. The water absorption rate was calculated according to formula (2) [14]:

$$Water\ absorption\ rate(\%) = \frac{m - m_0}{m_0} \times 100 \quad (2)$$

Where: m_o is the mass of the sample before immersion (g) and m represents the mass of the sample after immersion (g).

IV. Results and discussion

IV.1 Fourier-Transform Infrared Spectroscopy (FTIR)

The infrared spectral analysis was carried out on the PLA and the PLA/Alfa biocomposites having undergone hydrolytic aging. The use of the results obtained can lead to the study of the diffusion of water or interpretations concerning the different states of water and its interactions in the system after hydrolytic aging.

Figure 1 shows the IRTF spectra of (a) PLA, (b) PLA/Alfa, and (c) PLA/Alfa/2% BYK W-980 before and after 4320h (6 months) of immersion in distilled water at room temperature.

As shown in the figure, aged and not aged samples show the same absorption bands but with different intensities. This difference in intensity is a consequence of the effect of aging and the time of aging [15]. The spectrum of aged PLA (Figure 1 (a)) shows the appearance of an absorption band at 3650cm^{-1} due to the vibrations of the hydroxyl groups of the water molecules [16-18].

The same changes were detected for the biocomposites. However, we notice the appearance of a wide absorption band between 3000 and 3700 cm^{-1}, which increases in intensity after 4320 h of aging, reflecting the vibrations of elongation of the hydroxyls of the water molecules (OH) associated with the diffusion of the liquid within the matrix and the reinforcement/matrix interface [19]. The micro-voids formed in the biocomposites are the results of imperfect degassing during processing or of fiber/matrix decohesion. These micro-voids tend to accommodate water molecules [20]. Nevertheless, according to the literature, it is evident that hydrogen bonds occur [21]. It is generally accepted that the unbound water molecules are characterized by a peak around 3650cm^{-1} (case of PLA alone after aging) and that the bands between 3000cm^{-1} and 3700cm^{-1} characterize the associated water (case of biocomposites) [22]. These molecular interactions are also interpreted in the form of deformation vibration (HOH) although this mode of vibration is less sensitive to interactions of hydrogen bonds which give us less detail [16]. For untreated composites, Figure 1 (b) shows increased C-H and C = O absorption intensity for samples altered after 4320h. The increase in the carbonyl absorption band indicates certain changes in the structure of biocomposites due to chemical degradation [23]. In addition to the changes mentioned above, the spectra of the PLA/Alfa biocomposites in the absence of

BYK W-980, aged for 4320 hours, show a decrease in the intensity of the bands located in the 1300 and 900 cm^{-1} regions compared to the spectra of not aged biocomposites. This decrease is attributed to the cleavage of the C-O and C-O-C bonds of the untreated fiber and the hydrolysis of PLA under the effect of humidity [24, 25].

However, it can be observed a decrease in the absorption bands located in the regions 3500, 1600, 1001, and 600 cm^{-1}, after 4320 h of aging for the PLA/Alfa / 2% BYK W-980 biocomposites (Figure 1 (c)) but not for the PLA/Alfa formulation (Figure 1 (b)), this may be due to the decrease in micro-voids between the Alfa fiber and the PLA matrix as well as the hydroxyl groups on the surface of the fiber which are blocked by 2% BYK W-980, in other words, there are fewer hydrogen bonds.

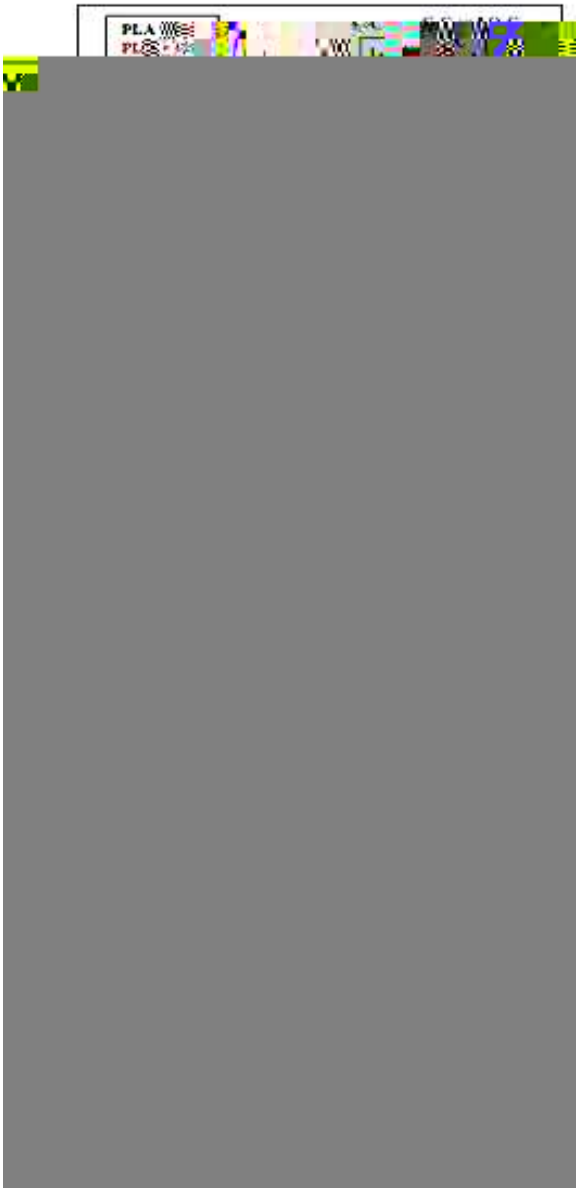

Figure 1. IRTF spectra of (a) PLA, (b) PLA / Alfa and (c) PLA/Alfa/2% BYK W-980 before and after 4320h of immersion in distilled water at room temperature.

IV.2 Thermo-Gravimetric Analysis (TGA)

The thermal decomposition of the three formulations PLA, PLA/Alfa and PLA/Alfa/2% BYK W-980 after aging was carried out by thermogravimetric analysis. Figure 2 shows the DTG thermograms of the three formulations.

The results indicate that the thermal stability of all samples decreased after hydrolytic aging. The decrease in this stability is proportional to the amount of water absorbed where it is found that the treated and untreated PLA

Alfa composites have undergone a strong decrease at temperatures T_5%, T_{50}% and T_{75}% which is quite expected because Alfa is very hydrophilic due to the hydroxyl groups it contains. The fibers act as paths for the diffusion of water into the biocomposite. So, the composite containing the fiber degrades more than the pure thermoplastic matrix [26, 27].

Also, the DTG curves clearly show a large decrease in the degradation rate of biocomposites compared to unfilled PLA as there is a peak shift towards lower temperatures. From the ATG thermograms of the different materials, we could derive the values of the decomposition temperatures at 5, 50, and 75% (T_5%, T_{50}% and T_{75}%, respectively) of mass loss (Table 1). From the results illustrated in the table below, it is noted that the two temperatures T_5%, T_{50}% and T_{75}% decrease after 4320 hours of immersion for the virgin PLA and the treated and untreated composites. This decrease may be due to the degradation of the fiber [19].

Table1. Degradation temperature of PLA, PLA/Alfa and PLA/Alfa/2% BYK W-980 biocomposites before and after immersion.

Temperature (°C)/ Formulations	PLA	PLA/Alfa	PLA/Alfa/2% BYK W-980
Before immersion			
T_5%	317	240	251
T_{50}%	356	306	315
T_{75}%	366	322	327
After immersion			
T_5%	296	238	201
T_{50}%	353	302	308
T_{75}%	363	315	320

Modification of PLA/Alfa biocomposites using 2% BYK W-980 influences thermal degradation behavior. The degradation temperature (T50%) and (T75%) (Table 1) of the modified biocomposite is shifted by approximately 6 °C. towards a higher temperature than that of the unmodified composites. Thus, this modification improved the thermal resistance. This effect is due to the stronger interaction between the fiber and the matrix with the formation of covalent bonds at the fiber-matrix interface and the good dispersion of the fibers [28].

The DTG thermogram showed degradation at 158 °C for PLA and at 178 °C for PLA/Alfa only present

in the aged samples (Figure 2), this is due to water absorption during immersion [29]. It is essentially free water that has filled the cavities of the material during ageing [30, 31].

The shift of the peak of the derivative towards the higher temperatures for PLA/Alfa compared to PLA also suggests the formation of bound water with the creation of bonds of higher energy between the water and the fiber [32]. It is interesting to point out the absence of this peak for PLA/Alfa/2% BYK W-980 composites. Indeed, a small quantity of OH bonds on the surface of the fibers induces a low level of humidity.

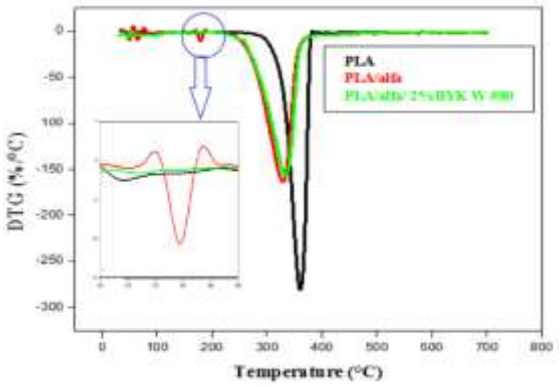

Figure 2. Thermogram DTG of PLA, PLA/Alfa and PLA/Alfa/2% BYK W-980 after 4320h of immersion in distilled water at room temperature.

IV.2 Water absorption test

Contact between a hydrophilic material and water molecules leads to the absorption of water by the surfaces and then in the volume of the material according to the laws of diffusion. According to various authors [33-36] the diffusion of water in biobased composites with an organic matrix is governed by different and successive mechanisms. First, the water molecules penetrate by capillary action between the polymer chains of the fiber and at the fiber/matrix interface, most often resulting from poor adhesion during the composite processing steps [33]. The water molecules then form hydrogen bonds with the hydroxyl groups of cellulose and hemicelluloses. Then, the water molecules diffuse at the interface and into the matrix [34,36]. At this level, some fiber components can also be hydrolysed, leading to decohesion at the fiber/matrix interface which may be responsible for the reduction of functional properties.

For each aging time, three samples: loaded and unloaded are weighed. The average mass gain values are shown in Figure 3. The mass variations of the PLA/Alfa biocomposites with and without BYK W-980 were related to the initial mass of virgin PLA to allow comparison with the unfilled matrix.

This Figure shows that the water uptake rate increases with increasing immersion time for all samples until saturation at about 180 days. As the PLA matrix does not show a significant gain in weight during this period of aging, we can therefore conclude that the penetration of water into the composites is through the reinforcement (Alfa fiber), the interface matrix/fiber, cracks and microspores that may exist on the surface of the composites that are probably formed during the manufacture of the biocomposites [19]. But still, the lower moisture absorption of PLA is expected due to its weaker hygroscopic nature compared to Alfa fiber. From the water absorption curves, it can be seen that the incorporation of the Alfa fiber into the PLA matrix caused a strong elevation in the rate of water absorption. They show a very high absorption rate (39%) compared to the virgin matrix (2.20%). Le Duigou et al. [37] evaluated the effect of immersion in distilled water at 23°C for two months of a PLA composite reinforced with 50% by mass of flax fibers on the evolution of its weight gain. While the weight gain of PLA alone does not exceed 0.5%, which of the composite increases with aging time to reach 14% after 8 weeks of aging.

This huge amount of absorbed water can be attributed to the presence of hydroxyl groups in the fiber structure. This is due to the low interfacial adhesion between the matrix and the fiber, in other words, due to the hydrophilic nature of the Alfa fiber caused by the large number of hydroxyl groups linked by hydrogen and Van der Waals bonds [38 ,39], which facilitates water insertion in PLA/Alfa biocomposites [40]. The authors explain the high water mass uptake for the composite by the high hydrophobicity and the structure of the flax fibres. The accessibility of water would also be influenced by the degree of esterification of the pectin, the size of the macromolecular chains of the hemicellulose as well as the crystallinity of the cellulose [41,42]. Other authors [43] have highlighted the influence of micro capillarity or lumen size on water diffusion. According to Okubayashi et al. [44] water can be absorbed by the hydroxyl groups of the fibers directly or indirectly. Directly, the water molecules would be easily absorbed on the hydroxyls present on the surface of the fibers or the hydroxyls of the amorphous zones. This “free” water would easily evaporate. Water molecules would also be absorbed on the inner surface of the voids and could thereby be trapped and bound to the fiber skeleton. These water molecules would be inserted between the cellulose chains, thus promoting their sliding relative to each other, causing the fibers to swell.

The introduction of BYK W-980 in the PLA/Alfa biocomposites decreased the water absorption rate from 39 to 15.91%. This improvement in the resistance to water absorption can be explained by the formation of bonds between the hydroxyl groups of the Alfa fiber and those of BYK W-980, which leads to the reduction of the hydrophilic character of the fiber. Indeed, the use of BYK W-980 reduces the diffusion of water in the PLA matrix reinforced by the Alfa fiber which is due to a better matrix/fiber

adhesion, therefore, reduction of micro-voids in the interfacial region as well as the hydroxyl groups which are blocked by the groups of carboxylic acids (BYK W-980) to form an ester.

According to Joseph et al. [45] the decrease in the water absorption rate can also be explained by the reorganization of the polymer chains and the migration of compatibilizers to the surface during the aging process. We have also noticed that from 150 °C, there is a slight declination of the curve which can be explained by the hydrolysis of PLA and consequently loss of mass.

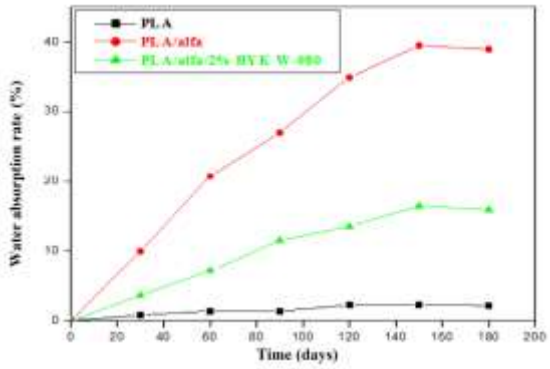

Figure 3. Evolution of the water absorption rate for pure PLA, PLA/Alfa and PLA/Alfa/BYK W-980 biocomposites

V. Conclusions

In this work, polylactic acid reinforced with Alfa fibers with and without the dispersing agent which is BYK W-980 underwent hydrolytic aging 4320 hours (180 days). Considering all the results, we were able to draw the following conclusions:

With the addition of vegetable fibers, greater degradation is observed. Thus, because of their hydrophobicity, the biocomposite obtained has a greater moisture uptake causing swelling at the fiber/matrix interface. This causes cracking and degradation by more significant chain cuts.

The presence of BYK W-980 influences the properties of biocomposites before and after immersion. These results are confirmed by measuring the weight gain which decreased in the presence of the dispersing agent. The latter reduces the number of hydroxyl groups in the fiber which are responsible for its hydrophilic nature and protects the fiber from degradation as seen in the Thermogravimetric Analysis results.

Conflict of interest. The authors report no conflict of interest.

References

[1] F. Heude, E. Richaud, E. Desnoux, X. Colin. A. General kinetic model for the photothermal oxidation of polypropylene. Journal of Photochemistry and Photobiology 29 6, 48-65, 2015.

[2] S. Dutta, S. De, B. Saha, Md. I. Alam. Advances in conversion of hemicellulosic biomass to furfural and upgrading to biofuels. Catalysis Science & Technology 2, 2025-2036, 2012.

[3] M.M. Kabir, H. Wang, K.T. Lau, F. Cardona. Chemical treatments on plant-based natural fibre reinforced polymer composites: An overview. Composites Part B: Engineering 43(7), 2883-2892, 2012.

[4] F. Signori, M-B. Coltelli, S. Bronco. Thermal degradation of poly(lactic acid) (PLA) and poly(butylene adipate-co-terephthalate) (PBAT) and their blends upon melt processing, Polymer Degradation and Stability 94(1), 74-82, 2009.

[5] J.D. Badia, L. Santonja-Blasco, A. Martínez-Felipe, A. Ribes-Greus. Hygrothermal ageing of reprocessed polylactide. Polymer Degradation Stability 97, 1881-1890, 2012.

[6] A. Arbelaiz, B. Fernández, J.A. Ramos, A. Retegi, R. Llano-Ponte, I. Mondragon. Mechanical properties of short flax fibre bundle/polypropylene composites: Influence of matrix/fibre modification fibre content, water uptake and recycling. Composite Science and Technology 65, 1582-1592, 2005.

[7] Z.N. Azwa, B.F. Yousif, A.C. Manalo, W. Karunasena. A review on the degradability of polymeric composites based on natural fibres. Material Design 47, 424-442, 2013.

[8] P. V. Joseph, M.S. Rabello, L.H.C. Mattoso, K. Joseph, S. Thomas, Environmental effects on the degradation behaviour of sisal fibre reinforced polypropylene composites, Composite Science and Technology 62, 1357-1372, 2002.

[9] D.F. Caulfield, D. Feng, S. Prabawa, R.A. Young, A.R. Sanadi. Interphase effects on the mechanical and physical aspects of natural fiber composites. Die Angewandte Makromolekulare Chemie 272, 57-64, 1999.

[10] T.T. Law, Z.A.M. Ishak. Absorption and dimensional stability of short kenaf fiber-filled polypropylene composites treated with maleated polypropylene. Polymers and Polymer Composites 21, 449-456, 2013.

[11] L. Mohammed, M.N.M. Ansari, G. Pua, M. Jawaid, M.S. Islam, A Review on Natural Fiber Reinforced Polymer Composite and Its Applications, International Journal of Polymer Science 2015, Article ID 243947, 1-15 2015. http://dx.doi.org/10.1155/2015/243947

[12] H. Ibrahim, D. Hammiche, A. Boukerrou, C. Delaite. Enhancement of biocomposites properties using different dispersing agents. Materials Today: Proceedings 36, 41-46, 2021.

[13] H. Ibrahim, A. Boukerrou, D. Hammiche. Effect of dispersant agent content on the properties of composites based on poly (lactic

acid) and alfa fiber. Macromolecular Symposia 395(1), 2000266, 2021.

[14] L. Klaai, D. Hammiche, A. Boukerrou, J. Duchet-Rumeau, J.F. Gerard, N. Guermazi. On the use of Prickly Pear Seed fibres as reinforcement in Poly Lactic Acid biocomposites. Journal of Emergent Materials, https://doi.org/10.1007/s42247-021-00288-1, 2021.

[15] F. Ahmad, H.S. Choi, M.K. Park. A Review: Natural Fiber Composites Selection in View of Mechanical, Light Weight, and Economic Properties. Macromolecular Materials and Engineering 300(1), 10-24, 2014.

[16] K. Hill, B. Swiecki, J. Cregger. The bio-based materials automotive value chain. Center of Automotive Research 1-92, 2012.

[17] C. Alves, P.M.C. Ferrão, A.J. Silva, L.G. Reis, M. Freitas, L.B. Rodrigues, D.E. Alves. Ecodesign of automotive components making use of natural jute fiber composites. Journal of Cleaner Production1 8, 313-327, 2010.

[18] D. Hammiche, A. Boukerrou, N. Guermazi, F. E. Arrakhiz. Effects of types of PVC-g-MA on wettability and dynamical behavior of Polyvinyl Chloride/Alfa composites. Materials Today: Proceedings 36, 10-15, 2021.

[19] M. John, S. Thomas. Biofibres and biocomposites, Carbohydrate Polymer 71, 343-364, 2008.

[20] A. Le Duigou, P. Davies, C. Baley. Seawater ageing of flax/poly (lactic acid) biocomposites. Polymer Degradation Stability 94, 1151-1162, 2009.

[21] H. Aouat, D. Hammiche, A. Boukerrou, H. Djidjelli, Y. Grohens, I. Pillin. Effects of Interface Modification on Composites Based on Olive Husk Flour. Materials Today: Proceedings, 36, 94-100, 2021.

[22] S. Isadounene, D. Hammiche, A. Boukerrou, D. Rodrigue, H. Djidjelli. Accelerated ageing of alkali treated olive husk flour reinforced Polylactic Acid (PLA) biocomposites: Physico-mechanical properties. Polymers and Polymer Composites, 26(3), 223-232, 2018.

[23] D. Rusu, S.A.E. Boyer, M.F. Lacrampe, P. Krawczak. Bioplastics and vegetal fiber reinforced bioplastics for automotive applications. Handb. Bioplastics Biocomposites Engineering Applied 397–449, 2011

[24] D. Hammiche, Alain Bourmaud, Amar Boukerrou, Hocine Djidjelli, Yves Grohens. Number of processing cycle effect on the properties of the composites based on alfa fiber. Journal of Thermoplastic Composite Materials 1-18, 2014.

[25] L. Soccalingame, D. Perrin, J.-C. Bénézet, S. Mani, F. Coiffier, E. Richaud, A. Bergeret. Reprocessing of artificial UV-weathered wood flour reinforced polypropylene composites. Polymer Degradation Stability 120, 313-327, 2015.

[26] D. Hammiche, Alain Bourmaud, Amar Boukerrou, Hocine Djidjelli, Yves Grohens. Number of processing cycle effect on the properties of the composites based on Alfa fiber. Journal of Thermoplastic Composite Materials 1-18 (2014).

[27] L. Klaai, D. Hammiche, A. Boukerrou, V. Pandit, Thermal and Structural Analyses of Extracted Cellulose from Olive Husk, Journal of Materials Today: Proceedings (2022), in press

[28] S. Panthapulakkal, M. Sain. Injection-molded short hemp fiber/glass fiber-reinforced polypropylene hybrid composites-Mechanical, water absorption and thermal properties. Journal of Applied Polymer Science 103, 2432-2441, 2006.

[29] T. Lundin, S.M. Cramer, R.H. Falk, C. Felton. Accelerated weathering of natural fiber filled polyethylene composites. Journal of Materials in Civil Engineering 16, 547-555, 2004.

[30] M.M. Kabir, H. Wang, K.T. Lau, F. Cardona. Chemical treatments on plant-based natural fibre reinforced polymer composites: An overview. Composites Part B: Engineering 43(7), 2883-2892, 2012.

[31] K. Hamad, M. Kaseem, F. Deri. Recycling of waste from polymer materials: An overview of the recent works, Polymer Degradation and Stability 98, 2801-2812, 2013.

[32] A. Bourmaud, C. Baley. Investigations on the recycling of hemp and sisal fiber reinforced polypropylene composites. Polymer Degradation and Stability 92, 1034-1045, 2007

[33] Z.N Azwa, B.F Yousif, A.C Manalo, W. Karunasena. A Review on the degradability of polymeric composites based on natural fibres. Materials And Design 47, 424-442, 2013.

[34] M.D.H. Beg, K.L. Pickering. Reprocessing of wood fibre reinforced Polypropylene composites. Part II: Hygrothermal ageing and its Effects. Composites Part A Applied Science 39(9), 1565-1571, 2008.

[35] V.S. Chevali, D.R. Dean, G.M. Janowski. Effect of environmental weathering on flexural creep behavior of long fibre-reinforced thermoplastic composites. Polymer Degradation and Stability 95, 2628-2640, 2010.

[36] H. Dhakal, Z. Zhang, M. Richardson. Effect of water absorption on the mechanical properties of hemp fibre reinforced unsaturated polyester composites. Composite Science and Technology 67, 1674-1683, 2007.

[37] A. Le Duigou, A. Bourmaud, C. Baley. In-Situ evaluation of flax fibre degradation during water ageing. Industrial Crops and Products 70, 204-210, 2015

[38] D. Hammiche, A. Boukerrou, H. Djidjelli, M. Beztout, S. Krim. Synthesis of a new compatibilisant agent PVC-g-MA and its use in the PVC/alfa composites. Journal of Applied Polymer Science 124, 4352-4361, 2012.
[39] S. Krim, A. Boukerrou, H. Djidjelli, J. Beaugrand, D. Hammiche. Reprocessing of the composites based on the polypropylene loaded with olive husk flour. Composites: Mechanics, Computations, Applications: An International Journal. 9, 163-187, 2018.
[40] A.H. Umar, E.S. Zainudin, S.M. Sapuan. Effect of accelerated weathering on tensile properties of kenaf reinforced high-density polyethylene composites, Journal of Mechanical Engineering Science 2, 198-205, 2012.
[41] G.C. Davies, D.M. Bruce. Effect of environmental relative humidity and damage on the tensile properties of flax and nettle fibres. Textile Research Journal 68, 623-629, 1998.
[42] C. Morvan, C. Andème-Onzighi, R. Girault, D.S. Himmelsbach, A. Driouich, D.E. Akin. Building Flax Fibres: More Than One Brick In The Walls. Plant Physiol. Biochemical Journal 41, 11-12, 2003.
[43] C.A.S. Hill, A. Norton, G. Newman. The water vapor sorption behavior of natural fibers. Journal of Applied Polymer Science 112, 1524-1537, 2009
[44] S. Okubayashi, U. Griesser, T. Bechtold. A kinetic study of moisture sorption and desorption on lyocell fibers. Carbohydrate Polymer 58 (2004) 293-299.
[45] P. V. Joseph, M.S. Rabello, L.H.C. Mattoso, K. Joseph, S. Thomas. Environmental effects on the degradation behaviour of sisal fibre reinforced polypropylene composites. Composite Science and Technology 62, 1357-1372, 2002.

Valorization of shrimp waste by chemical extraction of chitin and chitosan

Chadia IHAMOUCHEN[1*], Hocine DJIDJELLI[1], Amar BOUKERROU[1]
[1]*Department of Processes Engineering, Laboratory of Advanced Polymer Materials, University of Bejaia, 06000 Bejaia, Algeria*
Corresponding author: Chadia.benmerad@univ-bejaia.dz*
Received: 02 January 2022; Accepted: 26 January 2022; Published: 27 January 2022

Abstract

The aim of the present work is the recovery of co-products from shrimp shells by isolation of chitin and chitosan. Chitin is the major structural component of the exoskeleton of invertebrates. Chitosan, the deacetylated form of chitin, exhibits many biological activities including antifungal, antibacterial properties, wound-healing properties, and tumor inhibition. Its biological and physico-chemical properties make it an attractive biopolymer for highly targeted applications. The shrimp shells are widely used as raw material to isolate chitin, which is done by, the chemical or enzyme method. In this study, the choice is made on the first method which requires the dissolution of minerals, by acid treatment and extraction of the proteins by a basic treatment, followed by a stage of bleaching to remove pigments. Chitosan, it is obtained by deacetylation of chitin. The isolated substances were characterized by several techniques: chemical characterization, infrared spectroscopy (FTIR), differential scanning calorimetry (DSC) and the X-ray diffraction. FTIR analysis confirmed the conversion of chitin to chitosan with deacetylation of 78.7%. The presence of a high crystalline portion in the chitin was observed by XRD. Regarding the glass transition, the estimated humidity 6% of the chemical characterization in chitin played the role of a plasticizer; therefore, there was a decrease in Tg.

Keywords: *Chitin, Shrimp Shells, Chitosan, N-deacetylation*

I. Introduction

The oceans cover more than two-thirds of the earth's surface and a great diversity of organisms live and proliferate there. The management of marine litter is problematic. In the case of shrimp, more than 75% of its weight is rejected, the equivalent of more than 16,000 tons per year [1]. The management of this waste generates costs that affect the performance of processing companies.

There are many current solutions for the management of shrimp waste. some prefer burying or calcining, an expensive and environmentally harmful operation. Their transformation into compost, of course, is less polluting, but not profitable. Its use in animal feed, but expensive, unprofitable, and therefore little used. As a last resort, the discharge of this waste directly into the sea causes unwanted organic pollution [2].

The research studies on the recovery of shrimp waste led to the discovery of chitin. A major structural component of the exoskeleton of marine invertebrates, mainly crustaceans, is another route that appears to be more profitable, as this compound can be transformed into chitosan which has good commercial value [3]. Exhibits many biological activities including antifungal, antibacterial properties, wound-healing properties, and tumor inhibition. Their biological, physical, and chemical properties make it an attractive biopolymer for highly targeted applications

The objective of our work falls within the framework of the recovery and management of shrimp waste. The choice of this product lies in its richness in chitin. The physicochemical properties and the wide variety of biological activities make chitin and its derivatives the biopolymers of choice for many applications such as biotechnology, medicine, food, environment, etc... [4].

The recovery of chitin takes place in two stages: demineralization and deproteinization of the shells thus forming a protein matrix and containing insoluble mineral salts, mainly calcium carbonates. As for chitosan, it is obtained by deacetylation of chitin in 40% to 50% sodium hydroxide solution under pressure, at temperatures above 100 °C [5].

I.Material and methods

I.1. Shrimp shell powder

The shrimp shells were recovered at the port of Boumerdes, Algeria these shells have undergone several pre-treatment namely: Washing, Drying and Grinding

Figure 1: Shrimp shell before and after grinding

II. Experimental techniques

II.1. Chitin extraction process

Although chitin was identified before cellulose, it initially received less attention in scientific research than the latter. Chitin performs a function similar to that of cellulose in plants by acting as supportive and protective material. With its crystal structure and association with proteins, it prevents the internal organs of crustaceans from swelling in seawater [6]. Many methods have been developed to extract chitin from the shells of aquatic invertebrates. Chemical extraction consists of removing mineral elements (demineralization), proteins (deproteinization), and color (bleaching) [7].

a) Demineralization

Demineralization is carried out with 1N hydrochloric acid, for 30 min, at room temperature and with a solid/solvent ratio of 1/10 w/v, to transform the insoluble minerals of the shells into soluble salts. Calcium carbonate, the main mineral compound in the shell, reacts with HCl to form calcium chloride, water and carbon dioxide as described in the following reaction:

$$2\,HCl_{(aq)} + CaCO_{3_{(s)}} \xrightarrow{0} CaCl_{2_{(aq)}} + H_2O_{(l)} + CO_{2_{(g)}}$$

Most of the other minerals present react similarly and give soluble salts in the presence of acid. The salts formed can be separated from the chitin by simple filtration followed by washing. During the demineralization process, unwanted foams can form due to the production of carbon dioxide.

b) Deproteinization

The deproteinization is carried out in a reflux flask, in the presence of a 3% NaOH solution and with a solid/solvent percentage of 1/10 w/v. The duration of the basic treatment is of the order of 120 minutes at a temperature of 110 °C, to dissolve a larger part of the proteins.

c) whitening

For industrial applications, the chitin obtained from crustacean resources must be decolorized after the acid and alkali treatments. The bleaching was done in a solution of ethanol for 5 min with a solid/ratio of 1/15 w/v. Several washes are necessary between each step

II.2. Chitosan obtaining

While the extraction of chitin is easily achievable today, the most delicate step remains deacetylation, which requires sufficient substitution of the acetyl groups to result in chitosan. The chitin obtained is treated with a solution of sodium hydroxide (NaOH) 45% by mass at a temperature of 110 °C, for 1 hour and 30 minutes in a ratio of 1: 15w/v to remove some or all of the acetyl groups. The product obtained is then filtered, washed several times with distilled water and dried in an oven at 40 °C for 24 hours.

II.3. Characterization techniques

II.3.1. Chemical characterizations

a) Dry matter

1 to 2 g of sample is taken and weighed in a cup of known weight. The dish is placed for 24 h in an oven at 105 ° C, and then weighed after cooling for 30 min. The experiment is performed in triplicate [8, 9]. The dry matter content in chemical extraction products is given by the following formula:

$$DE(\%) = \frac{M_2 - M_0}{M_1 - M_0} .100$$

DE (%) is the part of dry extract, M_0 the weight of the cup, M_1 the wet weight, and M_2 the final dry weight.

b) Moisture content

The water content of the samples is determined according to the AFNOR standard (NF ISO 712). In a glass dish, previously dried for 1 hour in an oven at 100-105 ° C and cooled in desiccators, place 5 g of the product to be analyzed. Leave to dry in the oven at 100-105 °C until constant mass. Weigh the quantity of dry residue after cooling in desiccators [8, 9].

$$\text{Moisture}\ (\%) = \frac{\text{m (humid sample)} - \text{m (dry sample)}}{\text{m (humid sample)}} .100$$

c) Ash content

To determine the mineral content of the samples, approximately 1 g of the sample is weighed into a sheet of aluminum foil of known weight. It is folded up and placed in an oven for at least 5 hours at 600 ° C. After cooling, it is weighed again. The weight of

residual ash is equated with the mineral content. Each measurement is repeated three times [8, 9].

$$Ash\ (\%) = \frac{M_2 - M_0}{M_1 - M_0}.100$$

Ash% is the ash content, M_0 is the weight of the container, M_1 and M_2 are the weights before and after incineration respectively.

d) Purity and soluble residues

The purity of the product must be equal to or greater than 95%. Place 5 g of the sample to be analyzed in 100 ml of bi-distilled water and stir for 2 minutes. Filter after cooling through a tight filter. Evaporate the filtrate and dry at 100-105 ° C. The soluble matter content (SM %) must not exceed 5%. It is calculated using the following formula [3]. The degree of purity corresponds to the complementary part.

$$\text{SM}\ (\%) = \frac{\text{m (sample after drying)}}{\text{m (sample before test)}}.100$$

$$Purty\ (\%) = 100 - SM$$

II.3.2. FTIR spectroscopy Analysis

FTIR spectroscopy can highlight the appearance or disappearance of certain bands very significantly during extraction. The transmission spectra were carried out using an infrared spectrometer model SHIMADZU FTIR-8400S and were obtained in a wavenumber domain extending from 4000 to 400 cm^{-1} on KBr pellets, with a spectral resolution of 4 cm^{-1}.

II.3.3. Differential Scanning Calorimetry Analysis (DSC)

The apparatus used is of the TA Instruments, TGA Q10 type. The experiments were carried out on samples of mass ranging from 5 to 10 mg, placed in an aluminum crucible and heated in an inert nitrogen medium with a heating rate of the order of 10 °C/min and in a temperature range from 20 °C to 250 °C.

II.3.4. X-ray diffraction (XRD)

X-ray diffraction analyzes were performed on an X Pert Pro Panalytical type apparatus using the $K\alpha_1$ line of copper with wavelength λ = 1.540598 Å. The diffractograms were recorded from 0° to 70° (2θ) with a step of 0.01°.

The crystallinity index, denoted X (%), was calculated from the XRD spectra, according to the method of Focher et al. [10], according to the formula below.

$$X\ (\%) = \frac{I_{110} - I_{am}}{I_{110}}.100$$

With : I_{110}, (à 2θ = 20° dans le plan de réflexion (110)), Iam (autour de 2θ = 12°), le pic représentatif de la région amorphe

III.Results and discussion

III.1. Chemical characterizations

Chemical compositions such as dry matter content, moisture content, mineral or ash content, purities and soluble residues were determined for the chitin, and chitosan samples. Regarding the ash content, the test was carried out on the two samples chitin and chitosan in addition to the raw material (i.e without any prior treatment). The various results found are shown in Table 1.

Table 1: The chemical composition of the extraction products

Chemical compositions (%)	Chitin	Chitosan	Raw material
Dry matter	90,83	90,13	/
Humidity	6,5	5	/
Ash	0,24	0,24	28,54
purity	95,37	97,57	/
Soluble residues	2,43	4,63	

III.2. FTIR spectroscopy analysis

The FT-IR spectra of the chitin and chitosan samples are shown in Figure 2. From this Figure, we notice there are some absorption bands that are identical in the two spectra and other bands appear in the spectrum of chitin only whereas they disappear in that of chitosan [12].

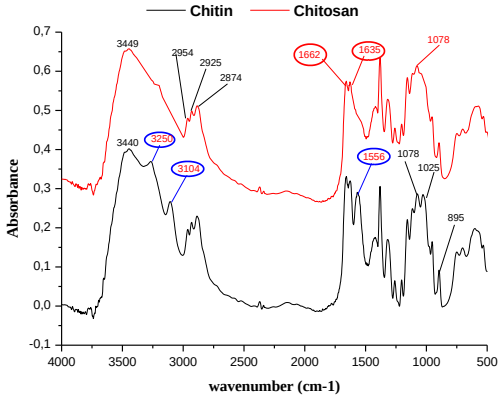

Figure 2: FTIR spectrum of chitin and chitosan

- The two spectra show a wide band between 3100-3500 cm^{-1} to more particularly at 3440 cm^{-1} which correspond to the –OH stretching vibrations
- The chitin spectrum also shows two peaks at 3250 and 3104 cm^{-1} which correspond to intermolecular hydrogen bonds and amide II –NH stretching vibrations. While these peaks do not exist in the spectrum of chitosan, which reflects a decrease in hydrogen bonds, therefore a more amorphous state is justified by the results of the XRD and that the deacetylation has taken place and has been successful.
- Peaks between 1960 -1860 cm^{-1} correspond to the stretching vibrations of –CH and $–CH_2$.
- The peaks appearing at 1662, 1635cm-1 and the peak at 1556 cm^{-1} in the chitin spectrum are due respectively to the C=O stretching vibrations of the groups in amide I and the amide II [13]. Thus, the appearance of two peaks at 1662 and 1635 cm^{1} shows that the chitin used is an α-chitin. However, α-chitin is the most stable and abundant orthorhombic system with aligned antiparallel macromolecules forming a regular crystal structure) [14]. The first peak corresponds to the vibrations between the C-N and C=O groups of the amide I linked by a hydrogen bridge to the OH groups. The second corresponds to an amorphous state, where the detected vibrations correspond to the bonds between the amide I and the C=O group [15].
- The absence of the peak at 1556 cm^{-1} in the spectrum of chitosan shows that the latter is very deacetylated [11].
- There are also two peaks at 1078 and 1025 cm^{-1} which correspond to the asymmetric C-O-C elongation vibrations of the glucosidic cycle and another peak at 895 cm-1 which corresponds to the β (1-4) glucosidic bonds in the polysaccharide.
- The absence of the peak at 1540 cm^{-1} which corresponds to the low or absence of protein impurities in the two spectra, demonstrates the purity of the chitin used and that the deproteinization was successful.

III.3. Degree of acetylation (DA) and degree of deacetylation (DD)

- The degree of acetylation (DA) is the one of the most important parameters to observe at the level of chitin is its degree of N-acetylation. The principle is based on the ratio of the areas between the characteristic bands of N-acetylglucosamine amine, chitin, and reference bands. According to the bibliography, several formulas are proposed [6]. In our case, we opted for the formula of M. R Kasaai et al. [16].

$$DA\ \% = \frac{\left(\frac{A_{1655}}{A_{3450}}\right)}{1{,}33}.100$$

With: A_{1655}: Absorbance of C=O groups in the amide. I A_{3450}: Absorbance of OH hydroxyl groups. The factor 1.33 represents the ratio (A_{1655}/A_{3450}) for a chitosan entirely N-acetylated.

- The degree of deacetylation (DD) is one of the main parameters characterizing chitosan, it corresponds to the degree of free $–NH_2$ groups in the chitosan molecule and is given by the following formula [16].

$$DD\ \% = NH2\ \% = [1 - DA\%].100$$

After carrying out the necessary calculations, we have got the following results.

Table 2: Degree of acetylation and deacetylation

sample	DA (%)	DD (%)
Chitin	82.59	37.90
Chitosan	28.25	78.7

From the values in Table 5, it can be seen that the deacetylation of the chitin gave an acceptable degree of deacetylation (DD ≈ 79%). This leads us to conclude that the chemical treatments carried out were very successful and allowed us to extract chitin and chitosan from the shell powder of the shrimp, similar to the commercialized products found on the market.

III.4. X-ray diffraction (XRD)

Figure 3 shows the XRD spectra of chitin and chitosan. X-ray diffraction spectra of chitin and chitosan show the presence of several peaks. Each peak is associated with an atomic plane; these planes

are designated by miler indices (h, k, and l). For example, the reflection at 2θ = 9.41°, is relative to the plane (020), the reflection at 2θ = 19.5° corresponds to the plane (110) and the reflection at 2θ = 26.40 ° is relative to the plane (130).

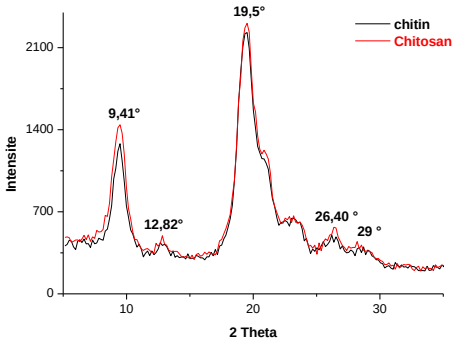

Figure 3: DRX spectrum of chitin and chitosan

It can be seen that the first two peaks (at 9.41 and 19.5°) are very intense and they correspond to the proportion of crystalline zones within the structure of the sample, and three other peaks at 12.82, 26.40 and 29° have very low intensities. Our results are similar to those obtained by Zhou et al. [17] with pure commercial chitin. Other researchers Entsar et al. [18]) have shown that α-chitin has a strong reflection at 2θ = 9-10° and 2θ = 20-21° and a minor reflection at 2θ = 26.4°. We can therefore conclude that the characteristic peaks of pure chitin appear in our sample prepared by chemical means. We also note that the intensity of the peaks corresponding to chitosan is slightly higher than that of chitin. The rate of crystallinity, denoted X (%), was calculated from the XRD spectra, according to the method of Focher et al. [10]. The results obtained are shown in Table 3.

Table 3: The rate of crystallinity of chitin, chitosan

Samples	X (%)
chitin	62,47
chitosan	54,46

According to the results of Table 3, it can be seen that the crystallinity index of chitosan which is 54.46% is lower than that of chitin which is estimated at 62.47%. This reduction, according to J. Machida [19], is attributed to prolonged acid and basic treatments which tend to reduce crystallinity as well as to deacetylation which involves the reduction of N-acetyl groups, demonstrated by Revol and Marchessault [20].

III.5. Differential enthalpy analysis (DSC)

Figures 4 show the DSC thermograms of the chitin and chitosan samples. We note that the two thermograms exhibit an endothermic peak between 100°C and 200°C which is due to the fusion of these two biopolymers, and more precisely the melting temperature of chitin was estimated at 198°C and that of chitosanis 186°C.This difference can be attributed on the one hand to the difference in the crystallinity rates [21], because a rate of 62.5% for chitin was recorded against 54.5% for chitosan calculated from the XRD. This result is confirmed by the heat of fusion ΔHf calculated from the DSC thermograms. On the other hand, the presence of impurity was estimated at 5% in chitin according to the chemical characterization carried out. This caused an increase in the melting temperature

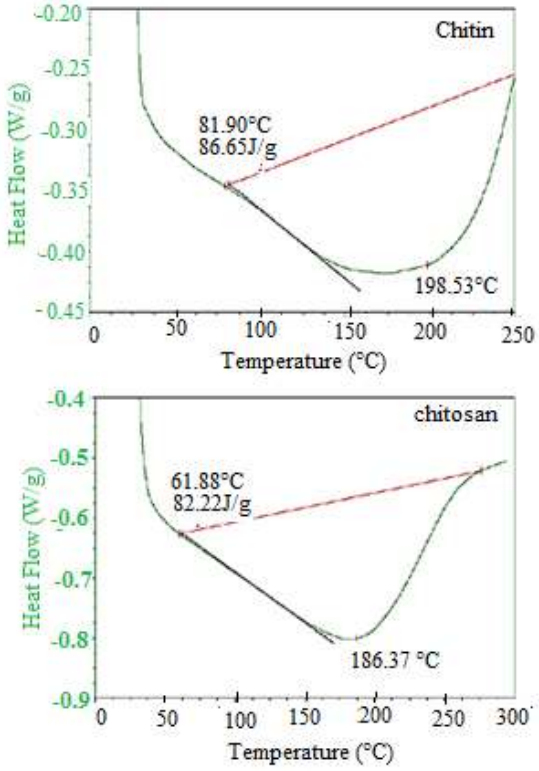

Figure 4: Representation of the melting temperature of chitin and chitosan

The glass transition temperatures (Tg) of chitin and chitosan are shown in Figures 5 and 6.

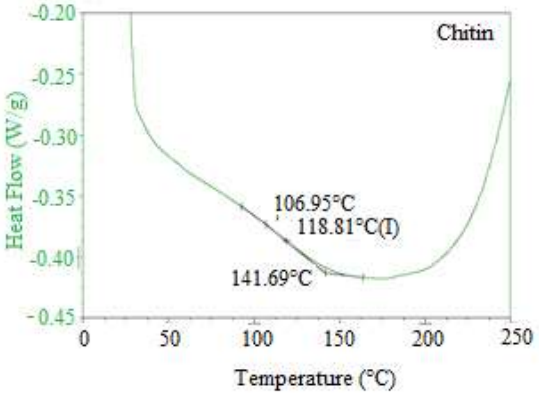

Figure 5: The glass transition temperatures of chitin

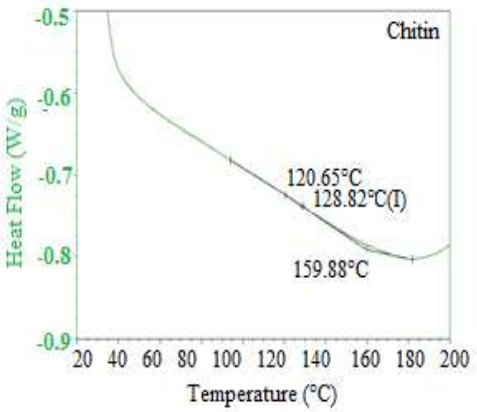

Figure 6: The glass transition temperatures of chitosan

In the chitin sample, its Tg is observed at 141°C.The decrease in the Tg of chitin compared to chitosan (160°C) would be due to the suppression of certain hydrogen bonds between the macromolecular chains, caused by the presence of a small quantity of water molecule (Rate ofhumidity estimated at 6.5% according to the results of the chemical characterization) which plays an important role as a plasticizer. Thus, increasing the flexibility of the chains, which makes their sliding a little easier.

IV. Conclusions

The demonstration of the extraction was examined by different analytical techniques, namely chemical characterization, IRTF analysis, X-ray diffraction and thermal analysis by DSC. The various results revealed that: The raw material exhibits a very high ash content of 28%, while the chitin sample registers only 0.24%. This means that the demineralization step was successful. IRTF analysis confirmed the conversion of chitin into chitosan, justified by the substitution of acetyl groups for chitin by amine groups for chitosan. The degree of acetylation and deacetylation for chitin (DA=82.59%) and chitosan (DD=78.7%) respectively, lead us to conclude that the chemical treatments carried out were successful and allowed us to extract chitin and chitosan similar to the commercial products found on the market. The presence of a large crystalline part in the chitin observed by XRD confirms the increase in the melting temperature of chitin (198 °C) compared to chitosan (186 °C) observed by DSC. Concerning the glass transition, the presence of water molecules estimated at 6% according to the results of the chemical characterization in chitin played the role of a plasticizer, thus increasing the flexibility of the chains that leads to sliding a little and consequently a reduction in his Tg.

Conflict of interest

The authors declare that they have no conflict for financial interests or personal relationships that how can influence the work reported in this paper.

References

[1] X. Xiong Chang, N. M. Mubarak, S. A. Mazari, A. S. Jatoi, A Ahmad, M. Khalid, R. Walvekar, E.C. Abdullah, R Rao Karri, M.T.H Siddiqui, S. Nizamuddin. A review on the properties and applications of chitosan, cellulose, and deep eutectic solvent in green chemistry. Journal of Industrial and Engineering Chemistry, 104, 362-380, 2021. https://doi.org/10.1016/j.jiec.2021.08.033

[2] M. Rinaudo, Chitin and chitosan: Properties and applications. Progress in Polymer Science. 31, 603-632, 2006 https://doi.org/10.1016/j.progpolymsci.2006.06.001

[3] M.N..V.R. Kumar. A review chitin and chitosan applications. Reactive and Functional Polymers. 46 (1), 1-27, 2000. https://doi.org/10.1016/S1381-5148(00)00038-9

[4] M. Abhinaya, R. Parthiban, P. Senthil Kumar, N. Vo Dai-Viet A review on cleaner strategies for extraction of chitosan and its application in toxic pollutant removal. Environmental Research 196, 110996, 2021. https://doi.org/10.1016/j.envres.2021.110996

[5] A. J. da Silva Lucas, E. Quadro Oreste, H. L. Gouveia Costa, H. M. Lopez , C D Medeiros Saad , C. Prentice. Extraction, physicochemical characterization, and morphological properties of chitin and chitosan from cuticles of edible insects. Food Chemistry 343, 128550, 2021. https://doi.org/10.1016/j.foodchem.2020.128550

[6] B. Taser , H. Ozkan, A. Adiguzel, T. Orak, M. Ozkan Baltaci, M. Taskin Preparation of chitosan from waste shrimp shells fermented with Paenibacillus jamilae BAT1. International Journal of Biological Macromolecules 183, 1191–1199, 2021. https://doi.org/10.1016/j.ijbiomac.2021.05.062

[7] D. Raabe, P. Romano, C. Sachs, H. Fabritius, A. Al-Sawalmih, S. B. Yi, G. Servos et H. G. Hartwig. «Microstructure and crystallographic texture of the chitinprotein network in the biological composite material of the exoskeleton of the lobster Homarus americanus». Materials Science and

Engineering:A 421, 143-153, 2006. https://doi:10.1016/j.msea.2005.09.115

[8] R. Priyadarshi, J.W. Rhim. Chitosan-based biodegradable functional films for food packaging applications. Innovative Food Science and Emerging Technologies 62, 102346, 2020. https://doi.org/10.1016/j.ifset.2020.102346

[9] M. Pakizeh, A. Moradi, T. Ghassemi Chemical extraction and modification of chitin and chitosan from shrimp shells. European Polymer Journal 159, 110709, 2021. https://doi.org/10.1016/j.eurpolymj.2021.110709

[10]. B. Focher, P.L. Beltrame, A. Naggi, G. Torri. Alkaline N-deacetylation of chitin enhanced by flash treatments. Reaction kinetics and structure modifications. Carbohydr Polym, 12(4), 405-418, 1990. https://doi.org/10.1016/01448617(90)90090-F

[11] C. Ben amar Chitosan: Properties, Modifications and Food Nanobiotechnology. Procedia Manufacturing 46, 652–658, 2020. http://creativecommons.org/licenses/by-nc-nd/4.0/.

[12] H. El Knidri, R. Belaabed, A. Addaou, A. Laajeb, A. Lahsini. Extraction, chemical modification and characterization of chitin and chitosan. International Journal of Biological Macromolecules 120, 1181–1189, 2018. https://doi.org/10.1016/j.ijbiomac.2018.08.139

[13] Q. Luoa, Y. Wanga, Q. Hana, L. Jib, H. Zhang, Z.Feib, Y. Wang. Comparison of the physicochemical, rheological, and morphologic properties of chitosan from four insects. Carbohydrate Polymers 209 (2019) 266–275. https://doi.org/10.1016/j.carbpol.2019.01.030.

[14] A. A.Vaidya, I.Hussain, M.Gaugler, D. A .Smith. Synthesis of graft copolymers of chitosan-poly(caprolactone) by lipase catalysed reactive extrusion. Carbohydrate Polymers 217, 98-109, 2019. https://doi.org/10.1016/j.carbpol.2019.03.081

[15] R. L. Lavall, O. B.G. Assis, P. Sérgio, F. Campana.β – Chitin from the pens of Loligo sp : Extraction and characterization. Bioresource Technology Vol.98, (13), 2465-2472. 2007. https://doi: 10.1016/j.biortech.2006.09.002

[16] M. R Kasaai. Various methods for determination of the degree of N-acetylation of chitin and chitosan: a review. J Agric Food Chem, 57(5),1667-76, 2009.https://doi:10.1021/jf803001m

[17] D Zhou, L. Zhang, S. Guo Mechanisms of lead biosorption on cellulose / chitin beads. Water Research 39(16), 3755-3762, 2005. https://doi:10.1016/j.watres.2005.06.033

[18] S. Abdou Entsar, S.A Nagy Khaled, Z.Maher Elsabee. Extraction and characterization of chitin and chitosan from local sources. Bioresource Technology 99(5), 1359-1367, 2008. https://doi.org/10.1016/j.biortech.2007.01.051

[19] J. Machida, S. Suenaga, M. Osada. Effect of the degree of acetylation on the physicochemical properties of α-chitin nanofibers. International Journal of Biological Macromolecules 155, 350–357, 2020. https://doi.org/10.1016/j.ijbiomac.2020.03.213

[20] J.F Revol, R.H Marchessaul. In vitro chiral nematic ordering of chitin crystallites. Int J Biol Macromol 15(6), 329-335, 1993. https://doi.org/10.1016/0141-8130(93)90049-R

[21] 21.21 H. Zhou, H. Tong, J. Lu, Y. Cheng, F. Qian, Y. Tao, H. Wang. Preparation of bio-based cellulose acetate/chitosan composite film with oxygen and water resistant properties. Carbohydrate Polymers 270 118381, 2021. https://doi.org/10.1016/j.carbpol.2021.118381

Prickly pear seed: from vegetable fiber to advanced applications: A review

Rebiha BELLACHE*, Dalila HAMMICHE, Amar BOUKERROU

Laboratoire des Matériaux Polymères Avancés, Département Génie des Procédés, Faculté de Technologie, Université de Bejaia, Algérie.

*Corresponding author** *rebiha.bellache@univ-bejaia.dz*
Received: 04 January 2022; Accepted: 24 January 2022; Published: 27 January 2022

Abstract

The prickly pear seed is a part rich in fatty substances; it can be exploited for the extraction of oils for food, cosmetic, pharmaceutical, and medical use. The focus of this review is to define one of the most expensive oils in the world "Prickly Pear Seed Oil" (PPSO). Its method of obtaining by cold pressing of its seeds makes it rich in active ingredients. For this, we will present a description of the cactus plant and its botanical classification, its chemical composition for either the pulp, the bark, or the seed. The morphology of the seed and its different applications, in addition to the seeds oil, presents extraordinary properties.

Keywords: *Prickly Pear Seed; Vegetable Fiber; Prickly Pear Seed Oil; Applications*

I. Introduction

The valorization of agricultural wastes for achieving lignocellulosic fillers (or fibers) represents a promising strategy to develop green materials with appropriate performance and high sustainability from an economic and ecological point of view [1].

The prickly pear (PP) or Opuntia ficus-indica (OFI), its scientific name comes from Latin Opuntius of Oponte; the name of the Greek city [2]. The common name is the cactus, which comes from the Greek word "kaktos", which means: the thorny plant [3]. According to Schweizer (1997), the plant may have a different name depending on the local idiom: Nopal, Tuna, African thistle, Prickly pear, El-tin-el-Choki, and others [2]. The Opuntia is native to Mexico, besides, the fruit of the prickly pear appears on the emblem of the Mexican flag [4]. It grows mainly in arid and semi-arid areas and extreme conditions. Its geographical distribution is located mainly in Mexico, Sicily, Chile, Brazil, Turkey, Korea, Argentina, and North Africa [5]. Low water exigency and a high water-use efficiency ratio favor the extension of cactus production, as underlined by the Food and Agriculture Organization [6].

Seeds constitute about 10–15% of the edible pulp and are usually discarded as waste after extraction of the pulp [7]. The oil processed from the seeds constitutes 7–15% of whole seed weight and is characterized by a high degree of unsaturation wherein linoleic acid is the major fatty acid (56.1–77%) [8]. According to Regalado-Rentería et al. (2018), this oil could be used in foods as a nutritional supplement, as well as an ingredient in cosmetics and pharmaceuticals. A major advantage is that the residual oilcake can be directly used in animal feed or other secondary products [9]. Edible cold-pressed oils are functional products because of their bioactive substances such as polyunsaturated fatty acids, tocopherols, sterols, phenols, carotenoids and chlorophyll. These oils have specific characteristics which provide additional health benefits [10].

The main objective of this review is to define prickly pear (PP), PPS and PPSO. Furthermore, to demonstrate the method of obtaining it by cold pressure of the prickly pear seeds (PPS) vegetable fiber, which is considered as food waste. In addition to this to make a valorization to its waste and to know the chemical compositions, physical and morphological characteristics, and the various applications of PPSO and PPS.

II. Botanical classification

Many authors have elaborated classifications of the genus Opuntia. The classification considered the most valid to date is undoubtedly that established by Britton and Rose in 1963 [11] :

- ✓ Kingdom : Plants.
- ✓ Order : Caryophyllalles.
- ✓ Subclass: Caryophyllidae.
- ✓ Family : Cactaceae.
- ✓ Group : Opuntiaeae.
- ✓ Genus : Opuntia.
- ✓ Subgenus : Platyopuntia
- ✓ Species: Opuntia ficus-indica, Opuntia megacantha.

The family Cactaceae has about 130 genus and 1500 species, of which 300 belong to the genus Opuntia [12].

The species of Opuntia the most widespread in Algeria are: Opuntia cylindrica, Opuntia mieckleyi, Opuntia vulgares, Opuntia schumanni, Opuntia megacantha, Opuntia maxima and Opuntia ficus indica [13].

III. Plant description

The prickly pear (PP) is a robust arborescent plant of (3 to 5 m) height, PP has a thick and woody trunk and an organization in flattened articles, of the elliptic or ovoid shape of green-mat color, having a length of (30 to 50 cm), a width of (15 to 30 cm) and a thickness of (1.5 to 3 cm) called cladodes or racquets. The cladodes ensure the chlorophyllic function and are covered with a waxy cuticle (the cutin) which limits the transpiration and protects them against predators [14].

The leaves are conical in shape and a few millimeters long, ephemeral, appearing on young cladodes, at their base are the areoles (about 150 per cladode) which are modified axillary buds.

The spines are whitish, solidly implanted, and long (1 to 2 cm). The glochids are fine spines of a few millimeters of a brownish color, easily detached, implanting themselves solidly in the skin [15].

The Opuntia bears flowers and fruits in abundance. The flowers are hermaphrodite; it is on the top of the rackets that appear beautiful and big lateral corollas, wide of (4 to 10 cm), of yellow to red color with all the intermediate nuances and become reddish with the approach of the senescence of the plant. In certain hot and arid regions the plant flowers and carries fruits twice in the year [2].

The seeds of the fruit are used to extract very valuable oil that is widely used in many fields. About 300 seeds for a 160 g of one fruit [16].

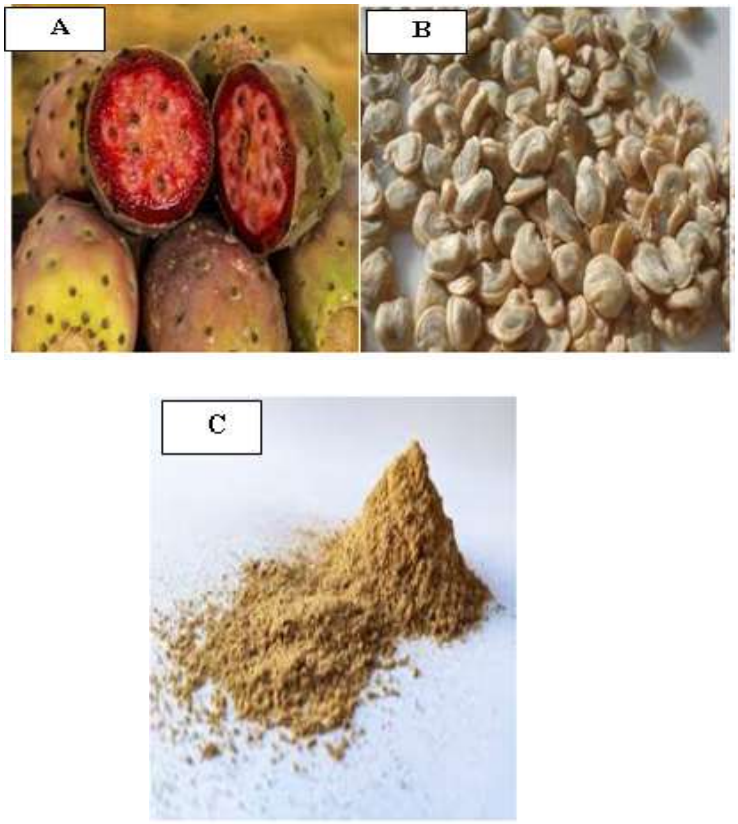

Figure 1: Prickly Pear Seed (A. Cactus, B Prickly Pear Seed, C. crushed Prickly Pear Seed)

IV. Chemical composition of Prickly pear (PP)

The (chemicals, minerals, vitamins and dietary fibers) compositions of prickly pear are summarized in the following tables.

Table 1: Chemical composition of prickly pear (g/100g of dry matter) [17]

Components	Pulp	Skin	Seed
Protein	0.5 – 5.3	8.3	11.8
Lipids	0.7 – 1	2.40	6.77
Total fiber	20.50	40.8	54.2
Ashes	0.4 – 8.5	12.10	5.90
Sugar	11 - 16	-	-

Table 2: Chemical composition of prickly pear of carbohydrate (% of dry matter) [17 - 18]

Sugar	Pulp	Skin
Sucrose	0.19	2.25 – 2.3
Glucose	29 – 35	14 – 21
Fructose	24 – 29.6	2.29 – 2.9

Table 3: Chemical composition of prickly pear of amino acids (mg/100g of dry matter) [19]

Amino acids	Pulp	Seed
Alanine	3.17	4.75
Arginine	1.11	6.63
Asparagine	1.52	Trace
Serine	6.34	8.46
Histidine	1.64	3.11
Glutamine	12.59	Trace
Methionine	2.01	0.70
Proline	46.00	Trace
Taurine	15.79	Trace

Table 4: Mineral composition of prickly pear (mg/100g of dry matter) [17]

Mineral elements	Pulp	Skin	Seed
Ca	163	2090	92 – 258
Mg	76	322	79 - 208
Na	7.8	<0.8	<0.8 – 12
K	559	3430	122 – 275
P	0.1	0.1	110 – 124
Fe	16.5	8.3	1.2 – 12.1
Cu	<0.8	0.9	<0.8 – 0.23
Zn	1.5	1.7	1.4 – 4.2
Mn	7	73	<0.8 – 2.3
Mb	<0.3	<0.3	<0.3

Table 5: Dietary fiber compositions of prickly pear (mg/100g of dry matter) [17]

	Pulp	Skin	Seed
Hemicellulose	2.5 – 6.4	20.8	9.9
Cellulose	14.2 – 2.24	71.4	83.2
Pectin	0.21 – 1.45	7.7	6.69
Lignin	0.01	0.06	0.19

Table 6: Vitamin compositions of prickly pear (mg/100g of dry matter) [19]

	Pulp	Skin	Seed
Vitamin K	53.2	109	52.5
Vitamin C	34 – 40	-	-
Vitamin E	527.4	2182	106

V. Prickly pear seeds (PPS)

V.1. Morphological description

According to the morphological analysis made by Habibi et al, (2004), the prickly pear seed consists of two layers: the pericarp is the outer layer of the seed and the endosperm is the layer located inside the seed [16].

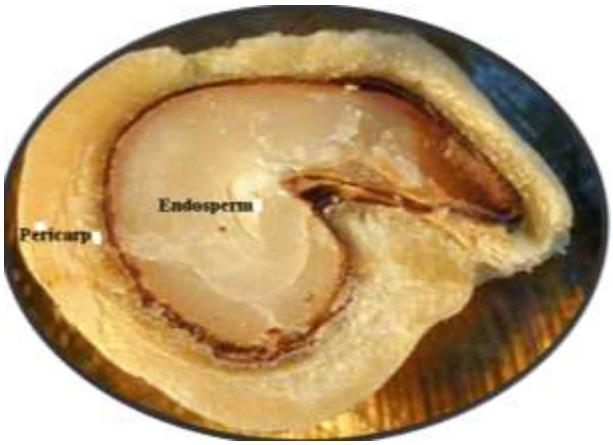

Figure 2: Cross section of the prickly pear seed PPS [16]

- ✓ **Pericarp:** there are two types of cells, mostly spindle fibers or sclerenchyma fibers and some spiral vessels. This support tissue is widely found in many cells such as fruit stones, spines and prickles of stems and leaves ... And what guarantees their thick walls is the regular layers of cellulose**.**
- ✓ **Endosperm:** it consists mainly of starch granules embedded in a tile-shaped parenchymatous cell wall.

V.2. Chemical composition of PPS

In recent years, many studies have multiplied to characterize the seeds of prickly pear and their constituents to assess their nutritional value.

Sawaya et al. [8] studied the composition of seeds, their potential uses in animal feed. They reported a protein content

of 16.6%, 17.2% of fatty substances, 49.6% of fiber and 3.0% of ash. The mineral content is high in sodium (67.6 mg 100 g-1), potassium (163.0 mg 100 g-1) and phosphorus (152.0 mg 100 g-1).

V.3. Prickly pear seed applications

Cerezal and Duarte [20] used the cactus pear pericarp to formulate marmalade. The seed meal seems to have potential use as a dietary fiber source for human consumption, for the extraction of oil.

Literature reports studies, several researchers have been working on prickly pear seed. PPS is used as a vegetable filler added to the polymer to strengthen its physic-chemical, mechanical, or thermal properties. As reported in the work of Malainine et al.[21] who was studied PPS / Poly(propylene) composites. And Scaffaro et al.[22] PPS was added to PLA, to prepare biocomposites by melt processing. Bellache et al. have incorporated the biodegradable polymer polyhydroxy (butyrate-co-valerate) with PPS to study the enzymatic [23] and hydrolytic [24-25] degradation of this biocomposite.

VI. Prickly pear seed oil (PPSO)

The prickly pear seed is a part rich in fatty substances; it can be exploited for the extraction of oils for food, cosmetic, pharmaceutical, and medical use.

Prickly pear seed oil (PPSO) belongs to the family of polyunsaturated oils like most vegetable oils. PPSO is a very rare and precious oil. Its yield is very low, there is only 6% oil in a small seed obtained by cold pressing, it must therefore treat about a ton of figs to obtain 1 liter of oil, a figure however variable depending on the parameters mentioned above but also the performance of the equipment used that is why this precious oil is very expensive.

Prickly pear seeds oil belongs to the family of polyunsaturated oils like most vegetable oils.

The commercial value of this oil is interesting because of its cosmetic characteristics sought. It is rich in unsaturated fatty acids such as linoleic acid (64.43%) and oleic acid (18.46%). Among the saturated fatty acids, the most important are palmitic acid (12.60%) and stearic acid (2.82%). On the other hand, its particularity lies in its richness in unsaponifiable matter (sterols and tocopherols). This characteristic could be a lever for its exploitation in the field of cosmetology, given the beneficial effects of these substances on the elasticity of the skin, cellular metabolism and restoration of the skin structure. It has remarkable cosmetic characteristics, as it prevents aging and wrinkles in the skin. The seeds are also used for the preparation of cream for dermal use.

An interesting content of polyphenols that are natural antioxidants and reduce the risk of cancer, cardiovascular diseases and neurodegenerative diseases such as Alzheimer's [26].

Conclusions

This review concludes that the vegetable fiber of prickly pear seeds has given much interest in recent years; Seed meal appears to have the potential for use as a source of dietary fiber for human consumption, and oil extraction and this latter present's one of the most expensive oils in the world.

Acknowledgments

The authors would like to thank ARAB MENOUI (Director of the company Thafath Tizi-Ouzou, Algeria) who provided us prickly pear seed.

Disclosure of interest: The authors report no conflict of interest.

References

[1] I. Benito-González, A. López-Rubio, M. Martínez-Sanz. Potential of lignocellulosic fractions from Posidonia oceanica to improve barrier and mechanical properties of bio-based packaging materials. Internationl Journal Biological Macromolecules. 118, 542-551, 2018.

[2] M. Schweizer. Docteur Nopal, le médecin du Bon Dieu. Clamecy ; PARIS (France). Imprimerie Laballery, p 81, 1997.

[3] M. S. Defelice. Prickly pear cactus, Opuntia spp. Aspinetingling tale. Weed Technology. 18, 869-877, 2004.

[4] H. A. Snyman. A greenhouse study of root dynamics of cactus pears, Opuntia ficus indica and O. robusta . Journal Arid Environments. 65, 529-542, 2006.

[5] J.P Rebman, and D.J. Pinkava. Opuntia cacti of North America: An overview Flor Entom. Florida Entomologist. 84(4), 474-482, 2001.

[6] G. Barbera, P. Inglese, et T. La Mantia. Seed content and fruit characteristics in cactus pear (Opuntia ficus-indica Miller). Science Horticultural. 58, 161‑165, 1994.

[7] F. C. Stintzing, A. Schieber, et R. Carle. Cactus pear, a promising component of functional food. Obst Gemüse und Kartoffelverarbeitung. 85, 40‑47, 2000.

[8] W. N. Sawaya, J. K. Khalil, M. M. Al Mohammad. Nutritive value of prickly pear seeds, Opuntia ficus indica. Plant Foods Human Nutrition. 33 (1), 91-97, 1983.

[9] E. Regalado-Rentería, J. R. Aguirre-Rivera, M.M. GonzálezChávez, R.Sánchez-Sánchez, F. MartínezGutiérrez, B.I. Juárez-Flores. Assessment of extraction methods and biological value of seed oil from eight variants of prickly pear fruit (Opuntia spp.). Waste Biomass Valor. 2018. https://doi. org/10.1007/s12649-018-0409-4 .

[10] D. Boskou. Edible cold pressed oils and their biologically active compounds. Journal of Experimental Food Chemistry. 3 (1), 1000e108, 2017.

[11] N.L Britton and J.N Rose. The Cactaceae. Vol 1 & 2, 1963.

[12] M. Mulas, G. Mulas. Potentialités d'utilisation stratégique des plantes des genres atriplex et opuntia dans la lutte contre la désertification. Short and Medium - Term Priority Environmental Action Programme, 2004.

[13] M. Arba. Les Opuntia fruits comestibles dans certaine région du Maroc. Dans IIème journée nationale sur la culture du cactus. El. Kelaa. DESS raghna-Maroc.2000.

[14] R.S. Wallace and A.C. Gibson. Cacti evolution and systematics. In: Cacti, Biology and Uses..University of California Press, Berkeley, California, United States of America. (Nobel, P.S. Ed.).1-21, 2002.

[15] S. Neffar. Etude de l'effet de l'âge des plantations de figuier de Barbarie(Opuntia ficus indica L. Miller) sur la variation des ressources naturelles (sol et végétation) des steppes algériennes de l'Est. Cas de Souk- ahras et Tébessa .thèse de doctorat en biologie végétale. Université Badji Mokhtar. Algérie. p 236, 2012.

[16] Y. Habibi. Contribution à l'étude morphologique, ultrastructurale et chimique de la figue de barbarie. Les polysaccharides pariétaux: charactérisation et modification chimique. Université Joseph-Fourier - Grenoble I, France, 2004.

[17] J. Aguilar Alejandra. Consumption of fruits and vegetables and health status of Mexican children from the National Health and Nutrition Survey 2012. Salud pública Méx. 56, 103-s112, ISSN 0036-3634. 2014.

[18] S. Nebbache, A. Chibani, R. Chadli and A. Bouznad. Chemical composition of Opuntia ficus-indica (L.) fruit. Africain Journal of Biotechnologie. 8 (8), 1623-1624, 2009.

[19] K. El-Mostafa , Y. El Kharrassi, A. Badreddine , P. Andreoletti , J.Vamecq , M. S. El Kebbaj, N. Latruffe , G. Lizard, B. Nasser, M. Cherkaoui-Malki. Nopal Cactus (Opuntia ficus-indica) as a Source of Bioactive Compounds for Nutrition, Health and Disease. Molecules. 19, 4879‑4901, 2014.

[20] P. Cerezal and G. Duarte. Use of Skin in the Elaboration of Concentrated Products of Cactus Pear (Opuntia ficus-indica (L.) Miller). Journal of the Professional Association Cactus Developement. 7, 61-83, 2005.

[21] M. E. Malainine, M. Mahrouz, et A. Dufresne, Lignocellulosic Flour from Cladodes ofOpuntia ficus-indica Reinforced Poly(propylene) Composites. Macromolecular Materials Engineering. 289 (10), 855‑863, 2004.

[22] R. Scaffaro, A. Maio, E. F. Gulino, et B. Megna, Structure-property relationship of PLA-Opuntia Ficus Indica biocomposites , Composites Part B: Engineering. 167. 199‑206, 2019.

[23] R. Bellache, D. Hammiche, A. Bettache, et A. Boukerrou. Enzymatic degradation of prickly pear seed (PPS)/ Polyhydroxy(butyrate-co-valerate) (PHBV) biocomposite. Materials Today: Proceedings. 2022, doi: 10.1016/j.matpr.2021.12.419.

[24] R. Bellache, D. Hammiche et A. Boukerrou. Physico-chemical characterizations of hydrolytic degradation of prickly pear seed (PPS)/Polyhydroxy(butyrate-co-valerate) (PHBV) biocomposite. Macromolecular symposia. 2022.

[25] R. Bellache, D. Hammiche et A. Boukerrou. Thermal and morphological analysis of hydrolytic degradation of prickly pear seed (PPS) enhanced Polyhydroxy(butyrate-co-valerate) (PHBV) biocomposite. Macromolecular symposia. 2022.

[26] Rapport du Ministere de l'agriculture et de la peche maritime. Etude du marché national et international des

produits issus du cactus (fruits frais, raquettes pour aliments de bétail, huiles) et l'exploration des opportunités offertes pour l'exportation. Midfac, 6-53, 2010.

Analytical stress solution in hyperelastic thick-walled sphere under external pressure using different strain energy functions

Abdelhakim Benslimane[1]*, Adel Benidir[2],
[1] *Laboratoire Mécanique, Matériaux et Energétique (L2ME), Département Génie Mécanique, Faculté de Technologie, Université de Bejaia, Bejaia 06000, Algérie*
[2]*Centre National d'Études et de Recherche intégrées du Bâtiment (CNERIB), Souidania-Alger 16097, Algérie*
**Corresponding author abdelhakim.benslimane@univ-bejaia.dz ; benslimane.ah@gmail.com*
Received: 03 January 2022; Accepted: 25 January 2022; Published: 30 January 2022

Abstract

Due to their large deformation, rubber-like materials are used in many industrial applications. However, few studies are available in the literature on the classification of rubber-like materials, their mechanical properties and the behavior of this material due to their hyperelastic and nonlinear behavior. In this work, an incompressible isotropic nonlinear elastic thick-walled spherical structure subjected to external pressure is studied using analytical formulation. The study aims to analyze the behavior and the stress field of such materials which are characterized by high deformability. Five different type strain energy functions are applied to a pressurized thick-walled hollow sphere to model the material behavior. A closed-form analytical solution is obtained and the results predicted from classic strain energy models (Neo-Hookean and Mooney Rivlin) and those obtained by Isihara, Biderman and Gent-Thomas models are compared in the prescribed case. The solution obtained, for different models, was used to determine the stress field (radial and hoop stresses) across thickness of the sphere. Finally, the influence of some parameters such as the radial pre-stretched sphere on stress components was examined. Comparisons are done to investigate the accuracy and evaluating the effectiveness of some existing constitutive models in the analysis of spherical vessel under external pressure.

Keywords: *Hyperelastic; Strain Energy Functions; Thick-Walled Pressure Vessel; Analytical Solution*

I. Introduction

Rubber and rubber-like materials which are assumed incompressible and isotropic materials are used in many engineering applications such as in automotive as tires, engine and transmission mounts, center bearing supports and exhaust rubber parts. The particularity of these rubber-like materials is their stress- stretch curves which are S-shaped to J-shaped forms due to their high deformability.

The mathematical modeling of such material encounters considerable difficulties related to their nonlinear behavior [1]. In recent years, many scholars have developed constitutive modeling of rubber like materials [1-5]. In order to describe the elastic behavior of elastomers, numerous models can be found in the prolific literature, but only few of them can be able to reproduce the response of the material, i.e. to satisfactorily fit experimental data for different loadings [6]. Among the various models recommended for the mechanical behavior of elastomers, the hyperelastic models are generally employed for modeling the nonlinear elastic behavior of homogeneous and isotropic polymers which exhibit large deformation [7-11]. The authors in [6] proposed a comparison of twenty different phenomenological and physical hyperelastic models for rubber-like materials. The material parameters of each model were determined by fitting to experimental data of [12]. The aim of their work [6] was to systematically compare hyperelastic models in order to classify them with respect to their ability to fit experimental data. There has been remarkable interest to know how an appropriate strain energy function can provide the foundation of an analytical solution on prediction of response of a realistic structure which undergoes three-dimensional large deformation.

The design of thin/thick-walled hollow spherical structures made of hyperelatic material and subjected to internal pressure remains a challenging talk. From a general perspective, cylindrical and spherical structures used in many industrial applications under internal and/or external pressure require rigorous stress analysis for their optimal, reliable and secure operational design. The behavior of an inflating of thin-walled cylindrical/spherical membrane under internal pressure has been investigated for large deformations by many authors [13-16]. In most cases the authors investigate the stability of hollow thin spherical membranes [17-19]. It is generally admitted that membranes and thin-walled spherical structures are successfully modeled as an ideal membrane with related mathematical simplifications.

However, in the case of thick-walled spherical structures the problem of formulation should consider the three-dimensional character of the solid. Accordingly, the analysis of the complete stress field of thick-walled spheres made of rubber-like materials by applying different hyperelastic models has received less academic interest.

In their work, Anssari-Benam [20] investigated the accuracy of a generalized neo-Hookean strain energy function to model

the two characteristic instability phenomena in the inflation of rubber-like.

Recently, Taghizadeh et al. [21] analyzed elastic behavior of cylindrical and spherical shells using different strain energy functions. The authors carried out an analytical study to investigate the stability of structures under internal pressure, where a comprehensive study was done on vanishing circumstances of the snap-through instability that occurs in the inflation of internally pressurized spherical shells and cylindrical tubes.

Debotton et al. [22] focused on axisymmetric bifurcations of thick-walled hollow spheres. The authors studied the mechanical behavior of a thick-walled spherical shell during inflation using four different material models. They investigated the existence of local pressure maxima and minima and the dependence of the corresponding stretches on the material model and shell thickness.

The present workplaces emphasis on the analytical formulation of the distribution of stresses across the thickness of thick-walled spherical structure subjected to external pressure. The analytical solutions are proposed for different constitutive models to study the inflation of a hyperelastic material as the material parameters are identified by using experimental calibration for various strain energy functions. In Section 2, the basic equations are developed for a sphere made of hyperelastic isotropic homogeneous material. Section 3 gives the results and the analysis of the sphere are described and discussed.

II. Mathematical formulation

We consider a hollow sphere made of an incompressible isotropic hyperelastic material. The sphere has inner and outer radii, noted A and B, respectively and subjected to an external pressure (labeled P_{out}). The schematic view of the thick sphere is shown in Figure 1, where the initial and the current configurations are detailed.

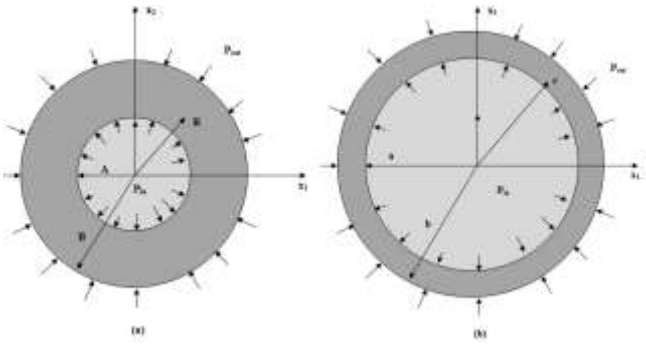

Figure 1 Thick-walled sphere with wall made of hyperelastic material, (a) initial configuration (b) current configuration.

Considering the symmetry of the geometry and the axisymmetric load conditions, it is more appropriate to consider a spherical coordinate system (r, θ, ϕ).

If (R, Θ, Φ) and (r, θ, ϕ) are coordinates of the rubber sphere before and after deformation respectively, the deformation pattern of the rubber sphere can be expressed as [5]:

$$r = f(R), \qquad \theta = \Theta, \qquad \phi = \Phi \tag{1}$$

Based on the theory of continuum mechanics, the deformation gradient tensor $\overline{\overline{F}}$ and left Cauchy green tensor $\overline{\overline{B}}$ are defined as [5]:

$$\overline{\overline{F}} = \overline{\overline{F}}^{T} = \begin{bmatrix} \lambda_r & 0 & 0 \\ 0 & \lambda_\theta & 0 \\ 0 & 0 & \lambda_\phi \end{bmatrix}, \quad \overline{\overline{B}} = \overline{\overline{F}}\,\overline{\overline{F}}^{T} \tag{2a, b}$$

Where λ_r , λ_θ and λ_ϕ are the principal stretches in the radial, circumferential and meridional direction of the thick-walled sphere. The stretches are expressed as follow [5]:

$$\lambda_r = \frac{dr}{dR}, \ \lambda_\theta = \frac{r}{R}, \lambda_\phi = \frac{r}{R} \tag{3}$$

Correspondingly, the principal invariants of the left Cauchy-Green strain tensor are [5]:

$$\begin{cases} I_1 = \mathrm{tr}\overline{\overline{B}} \\ I_2 = \dfrac{1}{2}\left(\left(\mathrm{tr}\overline{\overline{B}} \right)^2 - \mathrm{tr}\overline{\overline{B}}^2 \right) \\ I_3 = \det \overline{\overline{B}} \end{cases} \tag{4a,b,c}$$

Substituting Eq. (2) into Eq. (4) results in [5]:

$$\begin{cases} I_1 = \lambda_r^2 + \lambda_\theta^2 + \lambda_\phi^2 \\ I_2 = \lambda_r^{-2} + \lambda_\theta^{-2} + \lambda_\phi^{-2} \\ I_3 = \lambda_r \lambda_\theta \lambda_\phi \end{cases} \tag{5a,b,c}$$

For convenience [21]:

$$Q = \frac{R}{r} = \lambda_\theta^{-1} \tag{6}$$

It is worth noting that the present formulation based on the notation facilitates the steps and the derivation trend of the analytical solutions. It is considered that the material of the sphere is considered to be incompressible.

The resulting deformation is then described by the following equations [21]:

$$\lambda_r = Q^2, \qquad r^3 = R^3 + k \tag{7}$$

It can be easily concluded:

$$\frac{dQ}{dr} = \frac{Q^{-2} - Q}{r} \tag{8}$$

The principal Cauchy stresses are given in the form of:

$$\begin{cases} \sigma_r = \dfrac{Q}{2}\dfrac{\partial W}{\partial Q} - p \\ \sigma_\theta = \sigma_\phi = -Q\dfrac{\partial W}{\partial Q} - p \end{cases} \tag{9}$$

where the scalar p serves as an indeterminate Lagrange multiplier.
It can be also concluded:

$$\sigma_r - \sigma_\theta = \frac{3}{2} Q \frac{dW}{dQ} \tag{10}$$

where $W(Q) = W\left(Q^2, Q^{-1}, Q^{-1}\right)$

By considering nobody forces, the equilibrium equation of the axial symmetry in the current configuration can be achieved as:

$$\frac{d\sigma_r}{dr} + 2\left(\frac{\sigma_r - \sigma_\theta}{r}\right) = 0 \tag{11}$$

Applying the chain rule for finding derivatives, we have:

$$\frac{d\sigma_r}{dr} = \frac{d\sigma_r}{dQ}\frac{dQ}{dr} \tag{12}$$

The substitution of Eqs. (8) and (10) into equilibrium equation (11) could lead to :

$$\frac{d\sigma_r}{dQ} = -\left(\frac{3}{Q^{-3} - 1}\frac{\partial W}{\partial Q}\right) \tag{13}$$

The solution of Eq.13 can be computed easily by using any well-known computer algebra system such as Maple for different strain energy functions such as Neo-Hookean, Mooney-Rivlin, Gent-Thomas, Biderman and Isihara. These models have simple mathematical forms listed below:

- Neo-Hookean strain energy function [12]:

$$W_{NH} = C_{10}\left(I_1 - 3\right) \tag{14}$$

where $C_{10} = \mu/2$ and μ is the shear modulus.

- Mooney-Rivlin strain energy function [23]:

$$W_{MR} = C_{10}\left(I_1 - 3\right) + C_{01}\left(I_2 - 3\right) \tag{15}$$

where C_{10} and C_{01} stand for the material parameters of Mooney-Rivlin model.

- Gent-Thomas strain energy function [24]:

$$W_{GT} = C_1\left(I_1 - 3\right) + C_2 \ln\left(\frac{I_2}{3}\right) \tag{16}$$

where C_1 and C_2 are the two material parameters

- Isihara strain energy function [25]:

$$W_I = C_{10}\left(I_1 - 3\right) + C_{20}\left(I_1 - 3\right)^2 + C_{01}\left(I_1 - 3\right) \tag{17}$$

where C_{10}, C_{20} and C_{01} stand for the material parameters of Ishira model.

- Biderman strain energy function [26]:

$$\begin{aligned} W_B = {} & C_{10}\left(I_1 - 3\right) + C_{01}\left(I_2 - 3\right) \\ & + C_{20}\left(I_1 - 3\right)^2 + C_{30}\left(I_1 - 3\right)^3 \end{aligned} \tag{18}$$

where C_{10}, C_{01}, C_{20} and C_{30} stand for the material parameters of Biderman model.

The material parameters of each model can be identified using experimental data as shown by [6].

For example:
Gent-Thomas Model:

$$\begin{aligned} \sigma_r = {} & 3C_1\left(Q^4 + 4Q\right) \\ & + C_2\begin{pmatrix} \ln\left(1 + 2Q^6\right) \\ +2\sqrt{2}\arctan\left(\sqrt{2}Q^3\right) \end{pmatrix} + K \end{aligned} \tag{19}$$

where the parameter K in Eq. (19) is an unknown constant that is determined using the mechanical boundary conditions. Applying a constant uniform pressure at the outer surfaces of the thick-walled pressure vessel, the boundary conditions are expressed as:

$$\sigma_r\left(Q_{out} = \lambda_b^{-1}\right) = -p_{out} \tag{20}$$

$\lambda_a = a/A$ and $\lambda_b = b/B$ are the radial stretch at the inside and outside surfaces of the sphere, respectively and are expressed by:

$$\lambda_b^3 = \left(\lambda_a^3 - 1\right)\eta^3 + 1, \quad \frac{R}{r} = \frac{1}{\sqrt[3]{1+\left(\lambda_a^3 - 1\right)\frac{A^3}{R^3}}} \quad (21a, b)$$

where $\eta = A/B$

Here the hoop stress is obtained from Eq. (10):

$$\sigma_\theta = \sigma_\phi = \sigma_r - \frac{3}{2} Q \frac{dW}{dQ} \quad (22)$$

Assuming that the spherical shape of the pressurized sphere remains unchanged and $\Delta P = p_{in} - p_{out}$ is denoting the pressure difference between the inner and the outer surfaces:

$$\Delta P = -\sigma_r \left(Q_{in} = \lambda_a^{-1}\right) + \sigma_r \left(Q_{out} = \lambda_b^{-1}\right) \quad (23)$$

III.Numerical application

The calibrated material parameters for Gent-Thomas (W_{GT}), Ishira (W_{Is}), Biderman (W_B), Mooney Rivlin (W_{MR}) and for the neo-Hookean (W_{NH}) strain energy density functions are reported in Table 1.

Table 1 Parameters of hyperelastic models for Treloar experimental data [12].

Type of model	Material parameters
Neo-Hookean	C_{10} = 0.2
Mooney-Rivlin	C_{10} = 0.162 and C_{01} = 5.90 10^{-3}
Gent-Thomas	C_1 = 0.176and C_2= 5.65 10^{-2}
Ishihara	C_{10}=0.171, C_{20}=4.89 $10^{-3}$and C_{01}= -2.4 10^{-4}
Biderman	C_{10}= 0.208, C_{01}= 2.33 10^{-2}, C_{20} and C_{30} = -2.4 10^{-3}

The parameters of the models described by the strain density energy functions given in Eqs (14) to (18) are listed in Table 1 [6]. The parameters are derived by fitting data from the experimental results reported in Treloar [12].

In this section, we focus on the numerical results obtained for mechanical behavior modeling of these materials using five different types of strain energy density functions. These numerical computations are carried out for internal pressure and stress field.

We consider a thick sphere with the following characteristics: A = 0.1 m, B = 0.2m. In order to determine the unknown constants in these closed-form solutions, appropriate boundary conditions should be defined. The applied external pressure is P_{out} = 0.5 MPa.

IV.Results and discussions

IV.1. Validation

In order to validate the calculation methodology as well as the data consistency, the results reported in [21] are taken as a benchmark. In Figure 2, the pressure differences between the inner and the outer surfaces (ΔP) as a function of the stretch λ_a are plotted. The concordance between the outcomes of the current study and the reference (Taghizadeh *et al.* [21]) are evaluated by applying Mooney Rivlin (W_{MR}) and neo-Hookean (W_{NH}) strain energy density functions and by considering η = 0.35. The results from the current analytical formulation are in excellent agreement with those reported in [21]. In fact, the maximum error does not exceed 0.1%.

.

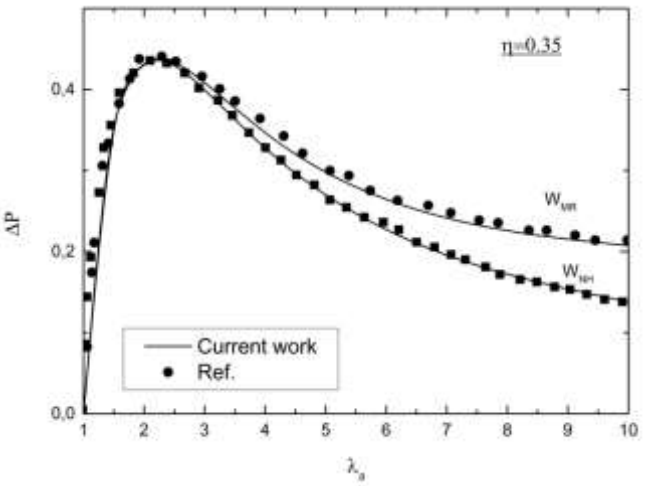

Figure 2 The pressure ΔP as a function of the stretch λ_a for the Mooney Rivlin (W_{MR}) and for the neo-Hookean (W_{NH}) strain energy density functions for η = 0.35: comparison of current results and results obtained by Ref. [21].

IV.2. Current work

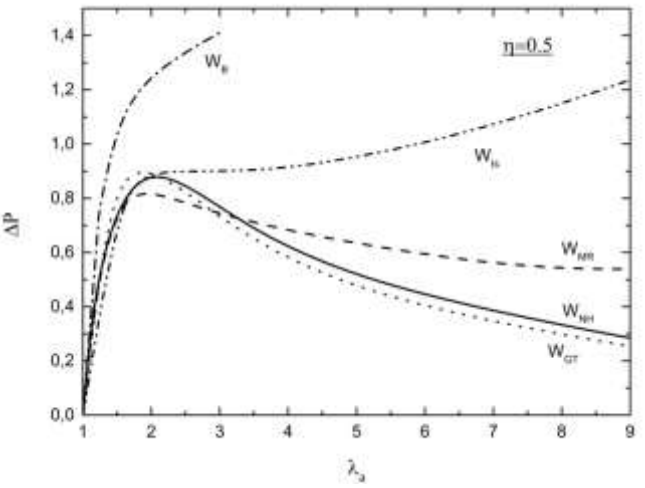

Figure 3. The pressure ΔP as a function of the stretch $\lambda_a$for the Gent-Thomas (W_{GT}), for the Ishira (W_{Is}), for the Biderman (W_B), for Mooney Rivlin (W_{MR}) and for the neo-Hookean (W_{NH}) strain energy density functions for η = 0.5.

Figure 3 illustrates the difference on the pressure ΔP as a function of the stretch λ_a for different strain energy density functions studied herein, for the case of internal to external radii ratios η = 0.5 for the spherical shell made of the rubber tested by Treloar (Treloar [12]). It could be concluded that a progressive increase of in the stretch λ_a leads to create a monotonic increase in pressure until $\lambda_a \sim 2$.

In the case of Gent-Thomas (W_{GT}), Mooney Rivlin (W_{MR}) and neo-Hookean (W_{NH}) models, the pressure curves have a single local pressure maximum and after that the pressure curves suddenly show monotonic decrease. This general observation is violated for the Ishira (W_{Is}) and the Biderman (W_B) models where the two curves remain with the same slope. Thus the evolution trend of the pressure could be classified as closer for three models whereas large dispersion is observed for the two representative curves of Ishira (W_{Is}) and the Biderman (W_B). In fact, as the stretch $\lambda_a$is higher than 2, a disproportional increase of the pressure is identified.

Figure 4a shows the radial stress distributions (σ_{rr}/P_i) in the *r*-direction for different strain energy functions, from which it is found that the radial stress components have its minimum values in at inner surface of the sphere $(r = A)$ and its magnitude shows a monotonic behavior increasing towards the outer surface of the sphere. However, for all the applied models, the normalized radial stress is minus one at outer surface ($\sigma_{rr}/P_i(r=B)$ = -1) of the sphere that satisfies the boundary conditions. The curves of the radial stresses components show a divergence between models results in the outer region of the sphere.
The circumferential stress component ($\sigma_{\theta\theta}/P_i$) is a maximum at the inner surface of the hollow sphere and its magnitude shows a monotonic behavior decreasing towards the outer surface of the sphere for all the tested strain energy functions (Figure 4b). The curves of the hoop stresses remain parallel.
As shown in Figure 4, the radial stress is consistently compressive; however, the hoop stress is tensile at the inner surface and become compressive at outer surface.

V. **Conclusions**

In this work, the behavior of a thick-walled pressure sphere made of an incompressible isotropic nonlinearly elastic material is studied. The aim through this investigation is to examine the stress field and the response of the sphere to the imposed mechanical loading. A closed-form analytical solution was derived from the governing equations. The hyperelastic behavior was modeled by employing five different strain energy functions (Neo-Hookean, Mooney Rivlin, Gent-Thomas, Biderman and Isihara) as established in the literature. The result analysis shows that an important divergence of the stress components is outlined as different models are applied. At the first glance, the study highlights the importance to impose a concise methodology to select modelsfor structural designing as hyperelastic materials are in process. The difference between the results obtained based on different strain energy functions are related to the accuracy with which these models reproduce the experimental data.
Mechanical loading as radial stretch is too important structural designing parameters; stress field of a thick-walled pressure sphere is examined in terms of the influence of these parameters. It was shown that the radial and hoop stress components are sensitive to the variation of radial stretch where the higher radial stretch is applied the higher stress components are generated.

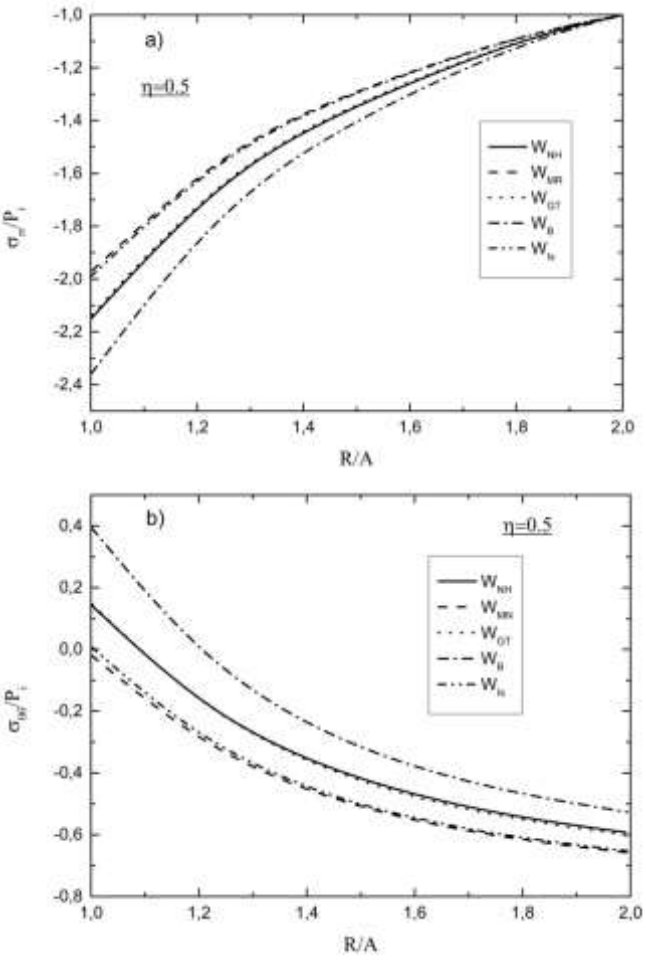

Figure 4. The normalized radial (a) and hoop (b) stresses as a function of the dimensionless radial position (R/A) of a spherical vessel made for the Gent-Thomas (W_{GT}), for the Ishira (W_{Is}), for the Biderman (W_B), for Mooney Rivlin (W_{MR}) and for the neo-Hookean (W_{NH}) strain energy density functions in the presence of radial loading λ_a =1.2 and for η = 0.5.

Acknowledgements

The author thanks the General Directorate of Scientific Research and Technological Development (DGRSDT/MESRS-Algeria) for their financial support.We would like to thank the anonymous reviewers.

References

[1] M.F. Beatty, Topics in Finite Elasticity: Hyperelasticity of Rubber, Elastomers, and Biological Tissues—With Examples. App. Mech. Rev., 40: 5, 1699 -1735, 1987. https://doi.org/10.1115/1.3149545

[2] R.S. Rivlin, Large elastic deformations of isotropic materials IV. Further developments of the general theory. Phil. Trans. R. Soc. Lond. A 241, 379-397, 1948. doi:10.1098/rsta.1948.0024

[3] R.W. Ogden. Nonlinear elasticity, anisotropy, material stability and residual stresses in soft tissue (lecture notes, CISM Course on the Biomechanics of Soft Tissue in Cardiovascular Systems), 65-108, 2003. CISM Courses and Lectures Series 441, Springer, Wien

[4] R.W. Ogden, Non-linear Elastic Deformations. Dover Publications, New York (1997)

[5] G.A. Holzapfel, Nonlinear Solid Mechanics. A Continuum Approach for Engineering. John Wiley & Sons, Chichester (2000)

[6] G. Marckmann, E. Verron. Comparison of hyperelastic models for rubber-like materials. Rubber Chemistry and Technology, American Chemical Society 79 (5), 835-858, 2006. https://doi.org/10.5254/1.3547969

[7] A.H. Muhr. Modeling the Stress–strain Behavior of Rubber. Rubber Chemistry and Technololgy 78, 391–425, 2005. https://doi.org/10.5254/1.3547890

[8] F. Elhaouzi, A. Nourdine, C. Brosseau, A. Mdarhri, I. El Aboudi, M. Zaghrioui. Hyperelastic Behavior and Dynamic Mechanical Relaxation in Carbon Black-Polymer Composites. Polymer Composites 40 (8), 3005-3011, 2018. https://doi.org/10.1002/pc.25142

[9] H. Shin, J. Choi, M. Cho. An efficient multiscale homogenization modeling approach to describe hyperelastic behavior of polymer nanocomposites. Composite Science and Technology 175, 128–134, 2019. https://doi.org/10.1016/j.compscitech.2019.03.015

[10] M.L. Ju, S. Mezghani, H. Jmal, R. Dupuis, E. Aubry. Parameter estimation of a hyperelastic constitutive model for the description of polyurethane foam in large deformation. Cellular Polymers 32(1), 21–40, 2013. https://doi.org/10.1177/026248931303200102

[11] A. Karimzadeh, M.R. Ayatollahi, S.S. Rahimian Koloor, A.R. Bushroa, M.Y. Yahya, & M.N. Tamin. Assessment of Compressive Mechanical Behavior of Bis-GMA Polymer Using Hyperelastic Models. Polymers 11, 1571, 2019. https://doi.org/10.3390/polym11101571

[12] L.R.G. Treloar, Stress-strain data for vulcanised rubber under various types of deformation, Transactions of the Faraday Society 40 59–70, 1944. https://doi.org/10.1039/TF9444000059

[13] E. Verron, R.Khayat, A. Derdouri, B. Peseux. Dynamic inflation of hyperelastic spherical membranes. Journal of Rheology. American Institute of Physics, 43, 1083-1097, 1999. https://dx.doi.org/10.1122/1.551017

[14] H. Alexander, Tensile instability of initially spherical balloons. International Journal of Engineering Science 9, 151–162, 1971. https://doi.org/10.1016/0020-7225(71)90017-6

[15] X. C. Shang. Tensile instability of nonlinear spherical membrane with large deformation. Applied Mathematics and Mechanics 12, 993–1000, 1991. https://doi.org/10.1007/BF02451485

[16] A.Goriely, M. Destrade, M. Ben Amar, Stability and bifurcation of compressed elastic cylindrical tubes. Quarterly Journal of Mechanics and Applied Mathematics 59, 615–630, 2006. https://doi.org/10.1016/J.IJENGSCI.2006.06.014

[17] D.M. Haughton, Y.C. Chen, Asymptotic bifurcation results for the eversion of elastic shells, Zeitschrift für angewandte Mathematik und Physik 54 (2), 191-211, 2003. https://doi.org/10.1007/s000330300000

[18] D.M. Haughton, E. Kirkinis. A Comparison of Stability and Bifurcation Criteria for Inflated Spherical Elastic Shells. Mathematics and Mechanics of Solids 8 (5), 561-572, 2003. https://doi.org/10.1177/10812865030085008

[19] D. M. Haughton, Inflation and bifurcation of compressible spherical membranes, Journal of Elasticity 12, 239–245, 1982. https://doi.org/10.1007/BF00042219

[20] A. Anssari-Benam, A. Bucchi, G. Saccomandi. Modelling the Inflation and Elastic Instabilities of Rubber-Like Spherical and Cylindrical Shells Using a New Generalised Neo-Hookean Strain Energy Function. Journal of Elasticity (2021). https://doi.org/10.1007/s10659-021-09823-x

[21] D. M. Taghizadeh, A. Bagheri, and H. Darijani. On the Hyperelastic Pressurized Thick-Walled Spherical Shells and Cylindrical Tubes Using the Analytical Closed-Form Solutions. International Journal of Applied Mechanics. 07(2015) No. 02, 1550027.

[22] G. deBotton, R. Bustamante, A. Dorfmann. Axisymmetric bifurcations of thick spherical shells under inflation and compression. International Journal of Solids and Structures, 50 (2), 403–413, 2013. https://doi.org/10.1016/j.ijsolstr.2012.10.004

[23] M.A. Mooney, A Theory of Large Elastic Deformation. Journal of Applied Physics, 11, 582-592, 1940. https://doi.org/10.1063/1.1712836

[24] A. N. Gent, & A. G. Thomas. Forms of the stored (strain) energy function for vulcanized rubber. Journal of Polymer Science 28, 625-637, 1958. https://doi.org/10.1002/pol.1958.1202811814

[25] A. Isihara, N. Hashitsume, & M. Tatibana, Statistical Theory of Rubber - Like Elasticity. IV. (Two - Dimensional Stretching). The Journal of Chemical Physics, 19 (12), 1508-1512, 1951. http://dx.doi.org/10.1063/1.1748111

[26] V. L. Biderman, Calculations of rubber parts (enrusse). RaschetinaProchnost, 40 (1958).

Development and validation of high-performance liquid chromatography assay method for simultaneous determination of Caffeic acid, Vanillin, and Cinnamic acid in Algerian propolis extract

Zahra TOUTOU[1, 2], Nacera CHIBANI[2], Lamia TAOUZINET[1, 3], Yasmina SALHI-AMRANI[1] and Sofiane FATMI[*1, 3]

[1] *Department of Processes Engineering, Faculty of Technology, Technology Pharmaceutical Laboratory, Université de Bejaia, 06000, Bejaia, Algeria.*

[2] *LMPA, Department of Process Engineering, Faculty of Technology, Université de Bejaia, Bejaia 06000, Algeria*

[3] *Faculty of Nature and Life Sciences, Associated Laboratory in Marine Ecosystems and Aquaculture, Université de Bejaia, 06000, Bejaia, Algeria.*

*Corresponding author** sofiane.fatmi@univ-bejaia.dz

Received: 01 January 2022; Accepted: 24 January 2022; Published: 30 January 2022

Abstract

Propolis is a natural bee substance and resinous material produced from various plants, which showed important biological activities. The current study aims to evaluate and validate simultaneous methods of identification and quantification of three phenolic compounds (caffeic acid, vanillin, and cinnamic acid) in propolis extract from different Bejaia regions using high performance liquid chromatography (HPLC). Chromatographic analyses were performed using gradient mode, in are versed-phase C-18 (150 x 4.6 mm, 5 µm) column. The mobile phase contained 0.5% v/v acetic acid in water (solvent A) and acetonitrile (solvent B), using a flow rate of 1 ml/min and by injecting 20 µl, at a wavelength of 290 nm. The method was validated according to ICH guidelines. Specificity, linearity, accuracy, precision, detection, and quantification limits studies were made. The results showed that the correlation coefficient (R2) was > 0.99 for Caffeic acid, Vanillin, and Cinnamic acid, the percentage of relative standard deviation (RSD) of all assays found below 2% and 5% for intra-day and inter-day, respectively, limits of detection were 0.024, 0.008, and 0.009 mg/ml and limits of quantitation was 0.074, 0.025, and 0,029 mg/ml, for Caffeic acid, Vanillin, and Cinnamic acid respectively. According to these various parameters: accuracy, precision, linearity, and specificity, the proposed method was successfully validated in the simultaneous assay of Caffeic acid, Vanillin, and Cinnamic acid.

Keywords: *High-Performance Chromatography, Simultaneous Validation, Natural Product, Polyphenol, Propolis Extract.*

I. Introduction

Propolis is a natural complex mixture collected and synthesized by bees from different plants (resins and waxes) and their salivary enzyme [1, 2]. It is used to construct, protect, and maintain the hives, and to treat many diseases in the poplar medicine [3].

Many studies revealed that propolis shows several pharmacological properties including anti-inflammatory [4, 5], antibacterial [6, 7], antioxidant [8], antiviral [9], and anticancer [10], this is due to the diversity of its chemical composition which depends on the bee species, meteorological conditions, plant, and geographical source [11].

The most important chemical contents of propolis are phenolic compounds which are considered secondary metabolites of plants, and they consist of wide large groups and classes that include flavonoids, terpenes, lignans, stilbene, aldehyde (vanillin), and phenolic acids [12].

Phenolic acids contain two main classes: hydroxycinnamic acids such as caffeic acid, cinnamic acid, and hydroxybenzoic acids like gallic acid [13, 14].

Different analytical methods were studied and applied in the analysis and quality assessment of propolis, among these chromatographic techniques: gas chromatography (MS), high performance liquid chromatography with diode array detection (HPLC-DAD) [15, 16], and high-performance liquid chromatography with Ultra-violet detector (HPLC-UV). Among the analytical methods, high-performance liquid chromatography (HPLC) [17, 18] is one of the most powerful analytical methods for this purpose. However, to ensure that analytical methodology is accurateusing (HPLC) methods, specific and over the specified range that an analyte will be analyzed; an analytical test method validation was completed. This validation, guidelines from the US Pharmacopeia (USP) and International Conference on Harmonization (ICH) [19].

The purpose of the present study was to develop and validate simultaneous method assay of Caffeicacid,Vanillin, and

Cinnamic acid in propolis extract from different Bejaia regions: Adekar, Akfadou, Baccaro, El kseur, Kendira, Kherrata, and Melbou, extracted by ultrasound and agitation methods. A simple HPLC method was used, allowing a good separation and short run time followed by a qualitative and quantitative determination of Caffeicacid, Vanillin, and Cinnamic acid.

II. Material and methods

Chemicals and reagents

Caffeicacid, Vanillin, Cinnamic acid,Alpha-tocopherol (vitamin E), Ascorbic acid (Vitamin C),Cholesterol was purchased from SIGMA-ALDRICH. Saturated phospholipids were purchased from RHONE POULENC (Phospholipon 90H lot: 90060). β-Cyclodextrin (β-CD) was obtained from Roquette Frères. Polyethylene Glycol 6000 (PEG 6000) was purchased from BIOCHEM.

HPLC-grade methanol, HPLC-grade acetonitrile, and acetic acid were purchased from BIOCHEM CHEMOPHARMA.

Equipment and Chromatographic conditions

Quantitative analysis of Caffeic acid, Vanillin, Cinnamic acid, vitamin E, vitamin C phospholipids, β-CD, and PEG 6000 were carried out using the high-performance liquid chromatography (HPLC) method, coupled to a UV detector set to 290 nm. HPLC-UV system (UltiMate 3000 RS-Variable Wavelength detector) was equipped with an auto-injector LC 1650, consisting of vacuum degasser, temperature-controlled well-plate autosampler, column thermostat, quaternary pump, and photodiode array detector. Chromatographic analysis was performed using a Hypersil ODS C-18 (150 x 4.6 mm, 5 µm particle size, 80˚A pore size column) from Thermo (Bellefonte, PA, USA). The mobile phase consisted of 0.5% v/v acetic acid in water (solvent A) and acetonitrile (solvent B), with a flow rate of 1 ml/min, injection volume was 20 µl, and the column temperature was 40°C as presented in Box 1. Vanillin, Caffeic acid, Cinnamic acid were identified by retention times and spectral data.

Box 1: Chromatographic condition of HPLC analysis.

Column: A reverse-phase C-18 (150 x 4.6 mm, 5 µm)

Mobile phase: 0.5% v/v acetic acid in water (solvent A), and acetonitrile (solvent B)

Flow rate: 1 ml/min

Detector: UV detector 290 nm

Injection volume: 20 µl

Mode: Gradient (90% solvent (A) at 0 min, 65% of solvent (A) at 5 min, 40% solvent (A) at 10 min, 20% solvent (A) at 15 min, 80% of solvent (A) at 20 min, and 90% of solvent (A) at 30 min)

Temperature: 40°C.

Standard preparation

The standard solution of Caffeic acid, Vanillin and Cinnamic acid were prepared in methanol in different concentrations: 0.0196-0.059 mg/ml, 0.0144- 0.0216 mg/ml, and 0.0392-0.059 mg/ml of Caffeic acid, Vanillin, and Cinnamic acid, respectively. These solutions were used to study linearity, accuracy, and precision. Specificity study was realized by the preparation of different solutions containing Polyethylene glycol 6000, β cyclodextrin, phospholipids 90H, Vitamin E, Cholesterol, and vitamin C.

Samples preparation

Propolis extracted from different regions was prepared in methanol at a concentration of 2mg/ml and analyzed by HPLC.

Method validation

Specificity

Specificity was determined by analyzing samples containing: Cyclodextrins, phospholipids, PEG 6000, methanol, mobile phase, mixer solution (containing all substances), cholesterol, ascorbic acid, and vitamin E and the sample solutions. All chromatograms were examined to determine if Caffeic acid, Vanillin, and Cinnamic acid co-eluted with any other excipient peak.

Linearity and range

Calibration standard was tested in the concentration range: 0.0196-0.059 mg/ml, 0.0144- 0.0216 mg/ml, and 0.0392-0.059 mg/ml of Caffeic acid, Vanillin, and Cinnamic acid, respectively. Five points of calibration were prepared at different concentration levels in methanol. Peaks areas (y-axis) versus drug (percentage) concentrations (x-axis) were plotted and subjected to regression analysis by the least-squares method, calibration equations $y = m x + a$ were obtained.

A method with r values higher than 0.99 can be considered linear. The range was an interval between the highest and lowest concentration analyte where acceptable linearity, accuracy and precision were obtained.

Accuracy

Accuracy was established by recovery studies at five concentrations: 0.0196-0.059 mg/ml, 0.0144- 0.0216 mg/ml, and 0.0392-0.059 mg/ml of Caffeic acid, Vanillin, and Cinnamic acid, respectively. At each level, samples were prepared in triplicate and recovery percentage was determined.

Precision

Precision was validated through intra-day and inter-day testing. The intra-day precision of the assay method was evaluated by carrying out five independent assays of Caffeic acid, Vanillin, and Cinnamic acid. Samples were against qualified reference standards on the same day and these studies

were repeated on three consecutive days to determine inter-day precision. Precision was expressed as % RSD of analyte concentration.

Quantitation Limit and detection limit

Quantitation limit (LQ) is the lowest amount of Caffeic acid, Vanillin, and Cinnamic acid, in a sample, which can be quantitatively determined with suitable precision and accuracy. The detection limit (LD) is the lowest amount of Caffeic acid, Vanillin, and Cinnamic acid in a sample that can be detected, but not necessarily quantitated as an exact value. Quantitation limit (LQ) and detection limit (LD) were determined based on the standard deviation of the response and the slope. The quantitation limit and detection limit are expressed as:

$$LQ = 10\ \sigma / S$$
$$LD = 3\ \sigma / S$$

Where σ is the residual standard deviation of the regression line, and S is the slope of the analyte calibration curve.

III.Results and discussion

HPLC method described was developed for simultaneous Caffeic acid, Vanillin, and Cinnamic acid quantification following International Conference on Harmonization (ICH) guidelines [19]. Specificity, Linearity, accuracy, precision, quantitation, and detection limit were tested to determine if the developed method is suitable for the identification and quantitation of Caffeic acid, Vanillin, and Cinnamic acid in propolis media. Retention time, plate number (N), and peak asymmetry factor (Tailing) were evaluated with the help of a standard chromatogram and shown in Table 1.

Table 1: System Suitability Parameters.

Parameters	Caffeic acid	Vanillin	Cinnamic acid
Tailing factor	1.1	1.36	1.05
No. of theoretical plate	80959	47937	176492
Retention time (min)	10.86	11.77	15.28

Method validation

Specificity

The specificity of the analytical method was determined by injection of 20µl: standard stock solution of Vitamin E and Cholesterol, β-Cyclodextrin, phospholipids 90H, PEG 6000, ascorbic acid, methanol, mobile phase, and solution contain all compounds. Chromatogram of Vitamin E and Cholesterol, β-Cyclodextrin, phospholipids 90H, PEG 6000, methanol, the mobile phase was not shown any significant peak at 10.86 min (caffeic acid retention time), 11.77 min (vanillin retention time), and 15.28 min (cinnamic acid retention time) (Figure 1, 2, and 3).

All compounds solution chromatogram (Figure 4) confirmed the absence of other peaks at the retention time of Caffeic acid, Vanillin, and Cinnamic acid.

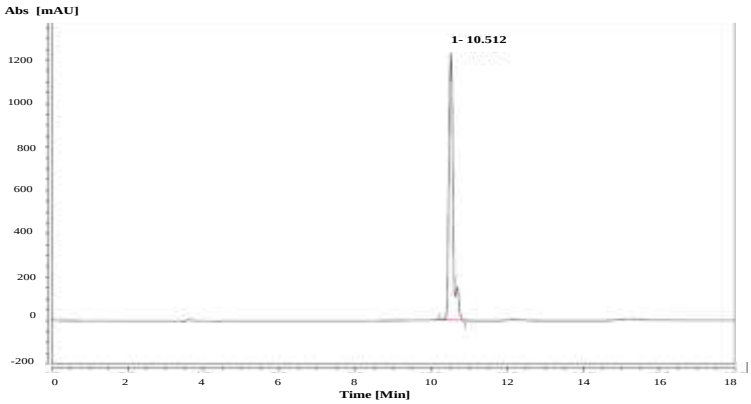

Figure 1: HPLC chromatogram of caffeic acid.

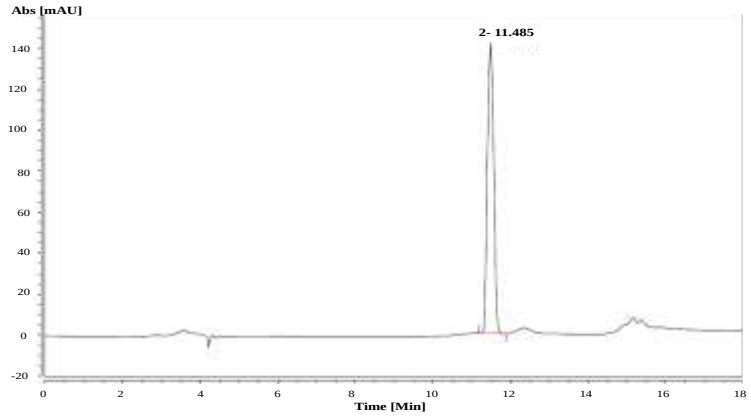

Figure 2: HPLC chromatogram of vanillin.

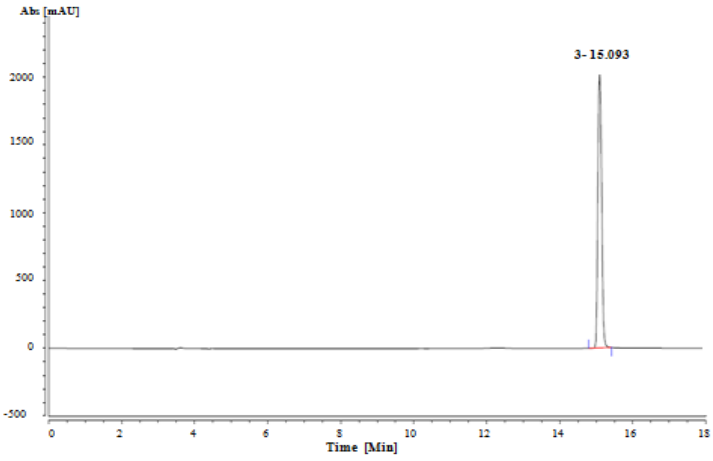

Figure 3: HPLC chromatogram of cinnamic acid.

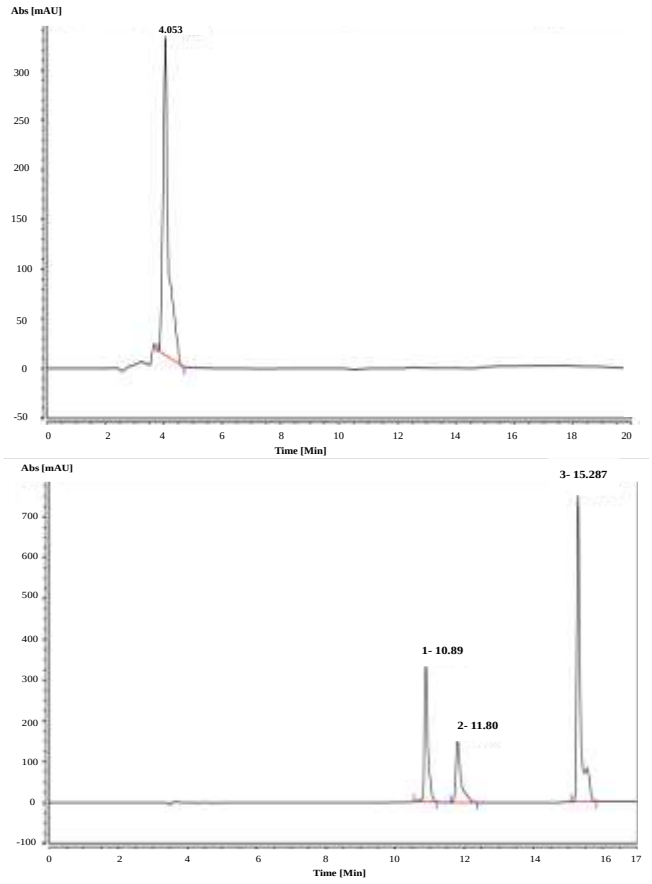

Figure 4: (A) Chromatogram of solution contains all compounds, and Chromatogram of Caffeic acid, Vanillin, and Cinnamic acid.

Linearity and range

A plot of peak area response against concentration is shown in Figure 5. Linearity was evaluated by calibration curves over the analytical range of 0.0196-0.059 mg/ml, 0.0144- 0.0216 mg/ml, and 0.0392-0.059 mg/ml of Caffeic acid, Vanillin, and Cinnamic acid, respectively (Table 2). Linear regression analysis for two reference compounds was performed by the external standard method. The correlation coefficient (R2) was found to be > 0.99 for Caffeic acid, Vanillin, and Cinnamic acid, indicating suitability for Caffeic acid, Vanillin, and Cinnamic acid, quantification. A great linear relationship was found for the two components (Caffeic acid, Vanillin, and Cinnamic acid). Results of linearity were presented in Table 2.

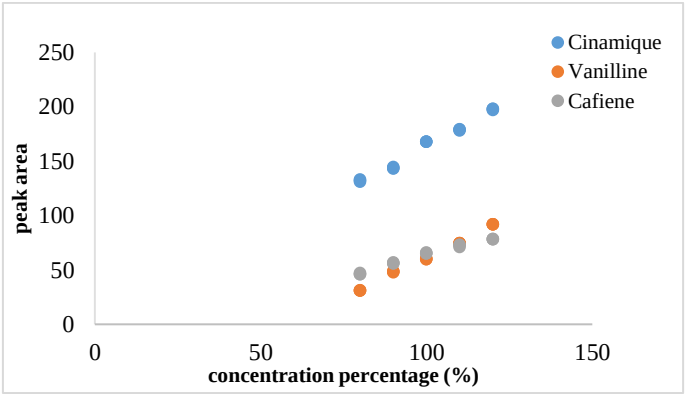

Figure 5: Calibration curve data for Caffeic acid, Vanillin , and Cinnamic acid.

Table 2: Calibration curve data for Vitamin E and Cholesterol.

Regression parameters	Caffeic acid	Vanillin	Cinnamic acid
Regression coefficient (R^2)	0.99		

Accuracy

To evaluate the accuracy and reliability of the method, recovery studies were carried out in the range of 80–120% concentration. Recoveries percentages were found to be average of 99.97%and 100% for Caffeic acid, Vanillin, and Cinnamic acid respectively. This method showed suitable accuracy. The obtained results are presented in Table 3.

Precision

The precision study has comprised the evaluation of the intra-day precision of the assay method. Five injections of target levels of calibration standard for Caffeic acid, Vanillin, and Cinnamic acid were performed. These studies were also repeated on three consecutive days to determine inter-day precision. The percentage of relative standard deviation (RSD) of six assay values was calculated and found to be below 2% and 5% for intra-day and inter-day, respectively. The results obtained are presented in Table 3. Thus, it concluded that it assures the precise HPLC method.

Table 3: Linearity, Precision and Recovery data for Caffeic acid, Vanillin andCinnamic acid**.**

Samples	Added standard (mg/ml)	Linearity (R2)	Accuracy (%recovery)	Precision (%RSD)		LD (mg/ml)	LQ(mg/ml)
				Intra-day	Inter-day		
Caffeic acid	0,039	0.997	97,81	0,670	9,298	0,024	0,074
	0,044		100,78				
	0,049		102,11				
	0,054		100,64				
	0,059		98,54				
Vanillin	0,032	0.997	99,57	0,049	3,116	0,008	0,025
	0,036		101,43				
	0,04		99,28				
	0,044		99,04				
	0,048		100,69				
Cinnamic acid	0,014	0.998	100,97	0,209	9,637	0,009	0,029
	0,016		97,60				
	0,018		102,25				
	0,019		98,98				
	0,022		100,21				

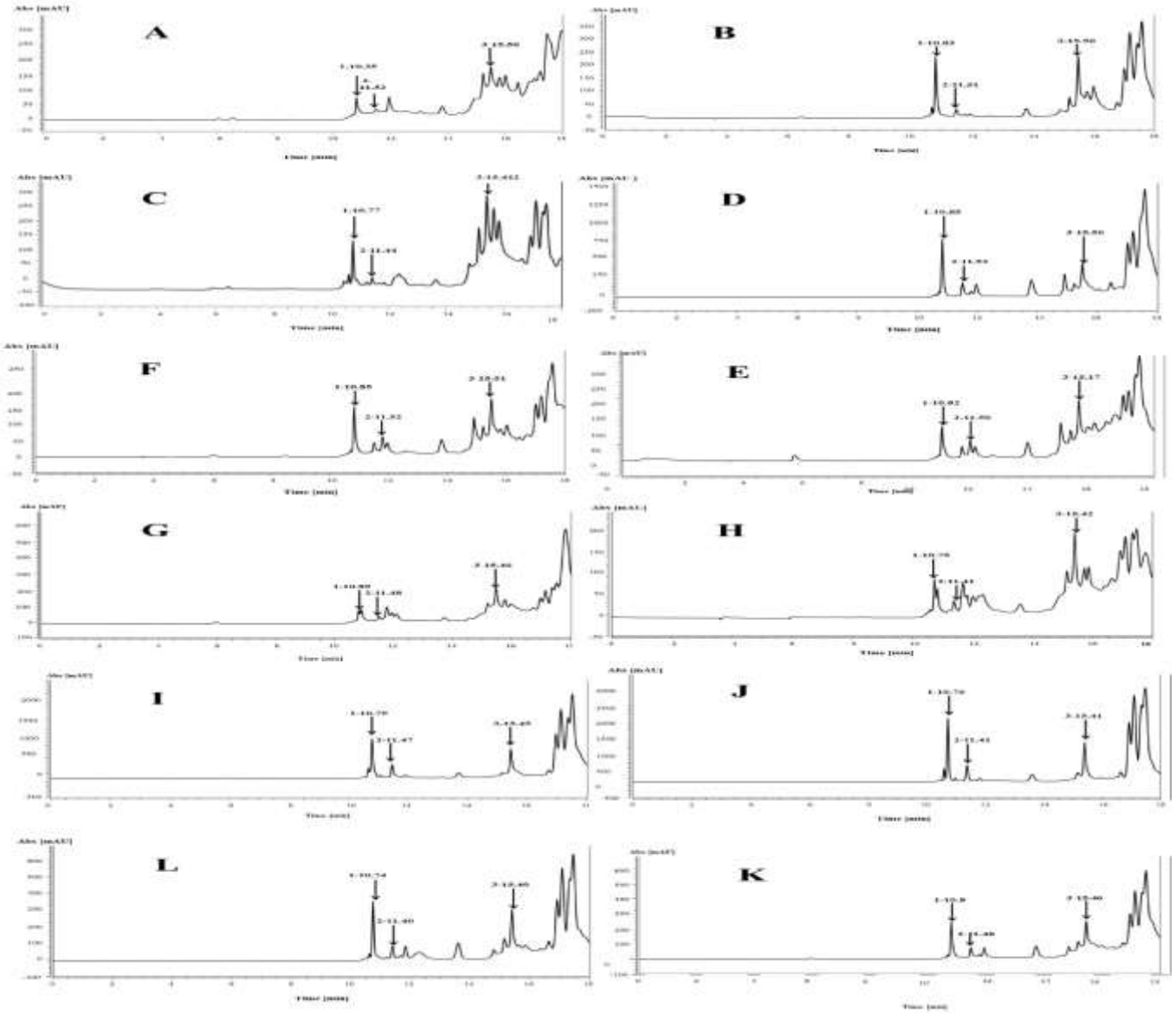

Figure 6: HPLC chromatograms of propolis extract from different Bejaia regions [A-Adekar(ultrasoundmethod),B-Akfadou (ultrasound method),C- Akfadou (agitataion method), D- Baccaro (ultrasound method),E- El kseur (ultrasound method), F- El kseur (agitataion method),G- Kendira (ultrasound method), H- Kendira (agitataion method), I- Kherrata (ultrasound method), J- Kherrata (agitataion method),K- Melbou (ultrasound method),L-Melbou(agitataionmethod),1-Caffeicacid,2-Vanillin,3-Cinnamicacid].

Detection and Quantitation Limits

Limits of detection and quantification were determined according to ICH, based on the standard deviation of the response and the slope. Caffeic acid, Vanillin, and Cinnamic acid presented limits of detection of 0.024, 0.008, and 0.009 mg/ml and limits of quantitation of 0.074,0.025, and 0,029 mg/ml, respectively. The results obtained are presented in Table 3 and indicated that the sensitivity of this HPLC method was suitable for the quantitative determination of Caffeic acid, Vanillin, and Cinnamic acid.

I.V. Conclusions

Analytical HPLC simultaneous assay of Caffeic acid, Vanillin, and Cinnamic acid was developed and validated satisfactorily for various parameters: accuracy, precision, linearity, and specificity as per ICH guidelines. This method shows simple, rapid, high precision and accuracy and offers the advantage of simultaneous assay of Caffeic acid, Vanillin, and Cinnamic acid in propolis extract from different Bejaia regions. Besides, this work offers an excellent alternative to methods already existing for Caffeic acid, Vanillin, and Cinnamic acid determination in propolis.

Acknowledgment*:*
The authors thank ‘Direction Générale de la Recherche Scientifique et Développement Technologique’, of Algeria for all the support provided.

Conflict of interest

The authors declare no conflict of interest, financial or otherwise.

References

[1] V.R. Pasupuleti, L. Sammugam, N. Ramesh, SH. Gan. Honey, Propolis, and Royal Jelly: A Comprehensive Review of Their Biological Actions and Health Benefits. Oxidative Medicine and Cellular Longevity 2017, 1-21, 2017. doi:10.1155/2017/1259510.

[2] X. Guo, B. Chen, L. Luo, X. Zhang, X. Dai, S. Gong. Chemical Compositions and Antioxidant Activities of Water Extracts of Chinese Propolis. Journal of Agricultural and Food Chemistry 59(23), 12610-12616, 2011. doi:10.1021/jf202818p

[3] S. El-Guendouz, S. Aazza, B. Lyoussi, et al. Effect of poplar-type propolis on oxidative stability and rheological properties of O/W emulsions. Saudi Pharmaceutical Journal 26(8), 1073-1082, 2018. doi:10.1016/j.jsps.2018.05.017

[4] S. Kiani, R. Birang, N. Jamshidian. Effect of Propolis mouthwash on clinical periodontal parameters in patients with gingivitis: A double-blinded randomized clinical trial. International Journal of Dental Hygiene 12550, 2021. doi:10.1111/idh.12550

[5] C. Marrassini, I. Peralta, C. Anesini. Comparative study of the polyphenol content-related anti-inflammatory and antioxidant activities of two Ureraaurantiaca specimens from different geographical areas. Chinese Medicine 13(1), 22, 2018. doi:10.1186/s13020-018-0181-1

[6] F. Zeighampour, F. Alihosseini, M. Morshed, AA. Rahimi. Comparison of prolonged antibacterial activity and release profile of propolis-incorporated PVA nanofibrous mat, microfibrous mat, and film: Research Article. Journal of Applied Polymer Science135(6), 45794, 2018. doi:10.1002/app.45794

[7] S. Bouchelaghem. Propolis characterization and antimicrobial activities against Staphylococcus aureus and Candida albicans: A review. Saudi Journal of Biological Sciences, 2021. doi:10.1016/j.sjbs.2021.11.063

[8] V. Curti, V. Zaccaria, A. TseteghoSokeng, et al. Bioavailability and In Vivo Antioxidant Activity of a Standardized Polyphenol Mixture Extracted from Brown Propolis. International Journal of Molecular Sciences 20(5), 1250, 2019. doi:10.3390/ijms20051250

[9] M. González, ME. García, A. Slanis, et al. Phytochemical Findings Evidencing Botanical Origin of New Propolis Type from North-West Argentina. Chem Biodivers 16(5), e1800442, 2019. doi:10.1002/cbdv.201800442

[10] M. Sahlan, Rizka NAlia Hapsari, K. Diah Pratami, et al. Potential hepatoprotective effects of flavonoids contained in propolis from South Sulawesi against chemotherapy agents. Saudi Journal of Biological Sciences 28(10), 5461-5468, 2021. doi:10.1016/j.sjbs.2021.08.022

[11] K. Salomao, AP. Dantas, CM. Borba, et al. Chemical composition and microbicidal activity of extracts from Brazilian and Bulgarian propolis. Letter in Applied Microbiology 38(2), 87-92, 2004. doi:10.1111/j.1472765X.2003.01458.x

[12] BAS. Machado, RPD. Silva, G. Barreto de A, et al. Chemical Composition and Biological Activity of Extracts Obtained by Supercritical Extraction and Ethanolic Extraction of Brown, Green and Red Propolis Derived from Different Geographic Regions in Brazil. Lightfoot DA, ed. PLoS ONE.11(1), e0145954, 2016. doi:10.1371/journal.pone.0145954

[13] D. Devequi-Nunes, BAS Machado, G. de A Barreto, et al. Chemical characterization and biological activity of six different extracts of propolis through conventional methods and supercritical extraction. Lightfoot DA, ed. PLoS ONE 13(12), e0207676, 2018. doi:10.1371/journal.pone.0207676

[14] H. Tugba Degirmencioglu, E. Guzelmeric, PI. Yuksel, H. Kırmızıbekmez, I Deniz, E Yesilada. A New Type of Anatolian Propolis: Evaluation of Its Chemical Composition, Activity Profile and Botanical Origin. Chem and Biodivers 16(12), 2019. doi:10.1002/cbdv.201900492

[15] M. Shahbaz, T. Zahoor, R. Arshad, et al. Chemical profiling, HPLC characterization and in-vitro antioxidant potential of Pakistani propolis collected from peripheral region of Faisalabad. Cellular and Molecular Biology (Noisy-le-grand) 67(1), 40, 2021. doi:10.14715/cmb/2021.67.1.6

[16] JA. Aldana-Mejía, GV. Ccana-Ccapatinta, VP. Ribeiro, et al. A validated HPLC-UV method for the analysis of phenolic compounds in Brazilian red propolis and Dalbergiaecastaphyllum. Journal of Pharmaceutical and Biomedical Analysis 198, 114029, 2021. doi:10.1016/j.jpba.2021.114029

[17] D. MKasote, MV. Pawar, RS. Bhatia, et al. HPLC, NMR based chemical profiling and biological characterisation of Indian propolis. Fitoterapia 122, 52-60, 2017. doi:10.1016/j.fitote.2017.08.011

[18] S. Kongkiatpaiboon, B. Vongsak, S. Machana, T. Weerakul, C. Pattarapanich. Simultaneous HPLC quantitative analysis of mangostin derivatives in Tetragonulapagdenipropolis extracts. Journal of King Saud University – Science 28(2), 131-135, 2016. doi:10.1016/j.jksus.2015.06.007

[19] International Conference on Harmonization (ICH), Validation of Analytical Procedures: Text and Methodology Q2 (R1), 2005.

Aging by burial in soil of polylactic acid biocomposites reinforced with Alfa fiber treated with dispersing agent

Lisa Klaai*[1], Dalila Hammiche[1], Hanane Ibrahim[1], Sonia Imzi [1], Amar Boukerrou[1]

[1]*Laboratoire des Matériaux Polymères Avancés (LMPA), Faculté de Technologie, Université de Bejaia, 06000 Bejaia, Algérie*

*Corresponding author** *lisa.klaai@univ-bejaia.dz*

Received: 06 January 2022; Accepted: 27 January 2022; Published: 30 January 2022

Abstract

Soil burial test comprises of placing samples in soil/ compost for long durations and testing the mechanical properties/dimensional changes/ morphology before and after soil burial. In a bioreactor, samples are placed in a composting vessel containing a mixture of compost and the percentage of biodegradation is theoretically calculated by measuring the amount of CO2 evolved from the composting vessel for a period of 45 days. This present work is focused on the study of the durability of different PLA/Alfa biocomposite materials treated with BYK W-980 and untreated, prepared via burial in soil aging. The study of biodegradation by burial in soil showed that the biodegradability of biocomposites prepared with untreated and treated PLA/Alfa degrade in soil more than those prepared with BYK W-980 for the same burial conditions. Knowing that the PLA buried in the ground is biodegradable after 4 to 5 years, by consecrating in this time interval of burial, we only have the fibers which degrade.

Keywords: *Aerobic biodegradation, Alfa fiber, Aging, Burial in soil, Dispersing Agent, Polylactic Acid.*

I. Introduction

Environmental concerns and awareness have paved the way to the development of biodegradable composites as a replacement for petroleum-derived or non-degradable polymers. So, there is an increase in demand for natural fiber-based composites for commercial use in various industrial Sectors [1].

A variety of biopolymers such as polylactic acid (PLA), polyhydroxyalkanoate (PHAs), and polybutylene succinate (PBS) are reported to be used as matrixes in composites. These biopolymers are naturally sourced and can potentially be combined with various natural fibres/lignocellulosic to produce biodegradable composites [2].

Natural fibers are sustainable materials in nature with advantages like low cost, lightweight, renewability, and, most importantly, biodegradability [3,4]. Pretreatment methods can improve the interfacial bonding quality. Physical treatment methods include hydrothermal treatment [5], microwave processing [6-8], steam explosion method [9], etc. Chemical treatment methods include acid treatment [10], alkaline treatment [11], acetylation treatment [12], benzoylation treatment [13], etc. Recently, many investigators have studied different pretreatment methods; the reports indicate that treated fibers can improve the physical and mechanical properties of fiber-plastic composites [14]. The rough surfaces of the fibers can easily combine with matrix (plastic), whereby the mechanical and thermal properties of the resulting composites are improved.

Several studies measure the biodegradation in biocomposites by means of soil burial test and testing in a bioreactor. Soil burial test comprises of placing samples in soil/ compost for long durations and testing the mechanical properties/dimensional changes/ morphology before and after soil burial. In a bioreactor, samples are placed in a composting vessel containing a mixture of compost and the percentage of biodegradation occurrence [5].

The influences of fiber content on microbial development as well as the preferential localization of microorganisms at the composite interface were analyzed by Feng et al. [15]. These authors evaluated the development of molds on HDPE composites reinforced with different mass rates of wood and bamboo fiber flour, the results obtained showed a progressive increase in the development of molds with the rate of fibers, with a better resistance for composites with wood fibres. By scanning electron microscopy, the authors observed a preferential concentration of mycelium in the interfacial zone between fibers and matrix of the composites. In addition, it appears that microbial growth has allowed a greater uptake of water mass.

In another study [16], PLA composites containing oil palm empty fruit bunch fiber was compounded with a slow releasing fertilizer and was subjected to soil burial tests at a temperature of 30°C and relative humidity of 80%. The samples were recovered at different stages of degradation and weighed to ascertain the mass loss during soil burial. The surfaces of the samples were also analyzed using scanning electron microscopy. The biodegradation rate of the samples

containing fibres and fertilizer was found to be lower than that of neat PLA. The scanning electron micrographs depicted the changes that occurred during the degradation period. The surface of the composite samples exhibited traces of shrinkage and roughness and exposed the natural fiber bundles. The scanning electron micrographs also revealed the presence of cracks and holes which were produced by the degradation of oil palm fibres. Soil burial test of biocomposites from wheat gluten and rubber wood sawdust were carried out by Bootklad et al. [17]. Compression molded samples were buried in soil for 15 and 30 days and the subsequent weight loss was measured. The authors observed that this type of green biocomposites could be degraded within 15 days. During the first 15 days, the weight loss was attributed to the leaching of glycerol which was used as a plasticizer in the system. The authors also observed that the biodegradation rate of composites containing 20 weight percent of rubber-wood waste was slower than that of wheat gluten biocomposites.

In another study, Pantyukhov et al. [18] investigated the biodegradation behavior of a range of lignocellulosic filler reinforced low-density polyethylene composites. The lignocellulosic fillers included flax shives, sunflower husk, hay, birch leaves, and banana skin. Soil mixture comprising of sand, garden soil, and horse manure were prepared and samples were placed in the soil for a period of 1year. The authors observed the greatest weight loss was in the case of hay filled composites followed by lignosulfonate, husk, banana, leaves, and shives. This was attributed to the chemical, fractional, and particle size composition of the fillers.

This present work is focused on the study of the durability of different PLA/Alfa biocomposite materials treated with BYK W-980 and untreated, prepared via burial in soil aging.

2. Material and methods

2.1. Materials

The polymer used in this work is Poly (lactic acid) (2003D grade) in the form of pellets. it was obtained from Nature Works LLC, USA. Alfa used as reinforcement was collected from the arid region of Algeria. The average particles size is <80 µm, obtained using a universal laboratory grinder for plastics and wood “VERDER”. The chemical composition of Alfa was reported previously [19].

Ethanol was 99% pure purchased from Changshu Yangyuan Chemical Company (Jiansu, China). The dispersing agent (BYK W-980) has been kindly given by BYK-CHEMIE whose properties are subjected previously [19].

The aging by burial in the ground of the samples prepared was carried out according to the ISO 14851 standard.

2.2. Methods

Fourier-Transform Infrared Spectroscopy (FTIR)

The IR spectra of olive husk powder and cellulose were analyzed with a Fourier transform infra-red (FTIR) spectrophotometer (SHIMADZU FTIR-8400S). The equipment was operated with a resolution of 4 cm^{-1} and scanning range from 4000 to 400 cm^{-1}. The samples were dried firstly at 80 °C for one hour before the FTIR analyzes.

Thermo-Gravimetric Analysis (TGA)

The thermogravimetric analysis (TGA) was performed on a DSC-LINSEIS calorimeter with a temperature range between 10 and 800 °C, with a heating rate of 10 °C/min under an inert atmosphere (nitrogen).

Aerobic biodegradation

The biodegradation of biocomposites was studied by burying different test specimens in the soil (compost) of a wild dump placed in pots of yoghurt. The latter was recovered from private compost in the Ouzellaguen/Béjaia region. Six specimens of each formulation were buried at a depth of 10cm for 3 months. All tests were carried out under aerobic conditions at a temperature of 20°C.

II. Results and discussion

Fourier-Transform Infrared Spectroscopy (FTIR)

Burial aging of no-charged and charged systems is accompanied by changes in their physical and mechanical properties. This is probably due to the structural changes that aging causes. Figure 1 shows the spectra of the different samples before and after 4320h buried in the ground. As shown in Figure 1, aged and unaged samples show the same absorption bands but with different intensities. The spectrum of aged PLA (Figure 1 (a)) shows the appearance of an absorption band at 35000cm^{-1} due to the vibrations of the hydroxyl groups of water molecules under the effect of humidity in the soil [20,21]. An increase in the intensity of the bands at 1543 and 719 cm^{-1} is also observed. This increase can be attributed to the presence of moisture during aging [22].

According to the spectra of aged samples, there is an increase in the absorption bands located in the 1800-1650cm^{-1} and 800cm^{-1} region due to the vibration of the water molecules. The increase in the hydroxyl absorption band can also be attributed to the hydrolysis of the ester [23] In addition, we observe on the spectra of the biocomposites (Figure 1 (b)) that after aging there is interference of the peaks of the hydroxyl groups with CH of CH_2, this can be explained by the fact that after aging, the humidity has diffused in the biocomposite, which created a broadening of the hydroxyl peak and its shift towards lower bands due to hydrogen bonds [24].

On the other hand, we can clearly observe a decrease in peak intensity in the OH stretch, the C=O stretch and the CO stretch indicating the absence of segregation between the PLA and the Alfa fiber, after 4320h of burial in soil, for

PLA/Alfa/BYK W-980 biocomposites (Figure 1 (c)), i.e., BYK W-980 reduced the hydrogen bonds between the matrix/fiber [25-27].

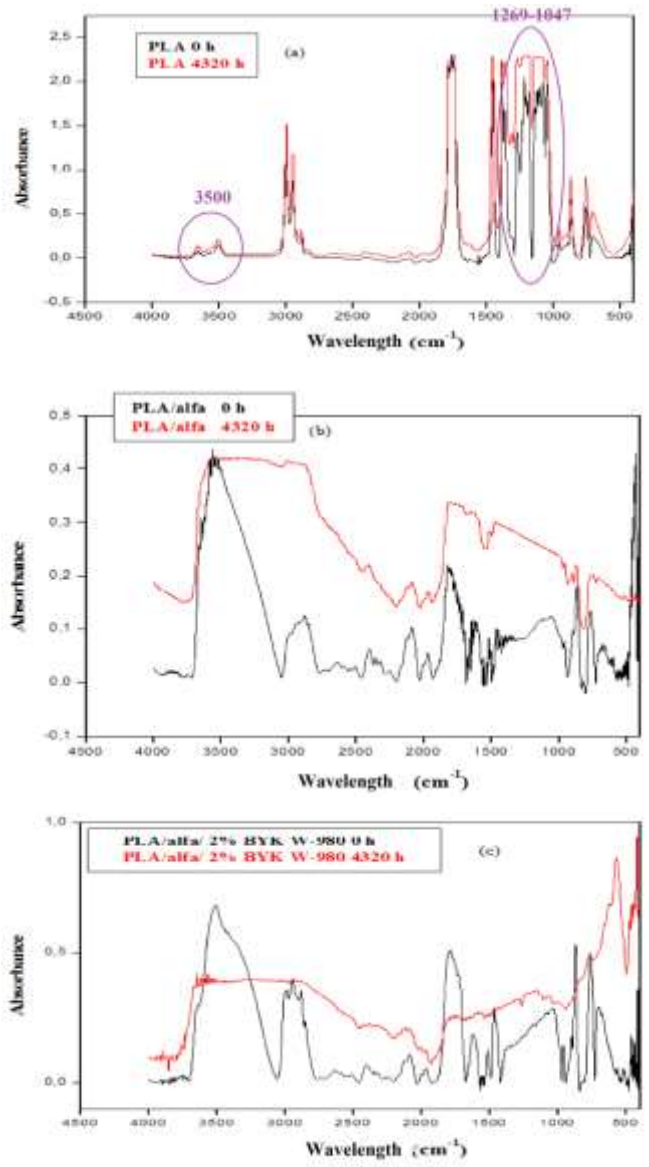

Figure 1: IRTF spectra of (a) PLA, (b) PLA / Alfa and (c) PLA / Alfa / 2% BYK W-980 before and after 4320h of burying.

Thermo-Gravimetric Analysis (TGA)

The thermal decomposition of charged and uncharged PLA before and after aging was carried out by thermogravimetric analysis (TG/DTG). From the TG thermograms of the different materials, it was possible to derive the values of the decomposition temperatures at 5, 50 and 75% ($T_{5\%}$, $T_{50\%}$ and $T_{75\%}$ respectively) of mass loss (Table 1).

Modification of PLA/Alfa biocomposites using 2% BYK W-980 influences the thermal degradation behaviour of the biocomposites. The degradation temperature at 50% mass loss ($T_{5\%}$) the TG curve of the modified biocomposite is shifted by approximately 120 °C. towards a higher temperature than that of the unmodified biocomposites. Thus, modification of PLA/Alfa biocomposites with BYK W-980 improved thermal stability. This effect is due to the stronger interaction between the fiber and the matrix with the formation of covalent bonds at the fiber/matrix interface [28].

Table1: Degradation temperature of PLA, PLA / Alfa and PLA/Alfa/2% BYK W-980 biocomposites before and after 4320h of burying

Temperature (°C)/ Formulations	PLA	PLA/Alfa	PLA/Alfa/2% BYK W-980
Before Burial			
T_5%	317	240	251
T_{50}%	356	306	315
T_{75}%	366	322	327
After Burial			
T_5%	286	213	225
T_{50}%	332	296	295
T_{75}%	342	317	310

Aerobic biodegradation

Biodegradation is followed by loss of mass from samples buried in soil, which is due to assimilation of the material by microorganisms [29]. Figure 2 shows the mass loss of PLA and the various biocomposites during 180 days of burial in the ground.

According to figure 2, it is noted that the loss of mass of virgin PLA is almost zero whatever the time of burial in the ground, in this chosen interval. Knowing that PLA buried in the ground is biodegradable after 4 to 5 years, only the fibers degrade [30]. We can also note that the mass loss of PLA/Alfa is much higher than PLA/Alfa/2%BYK W-980. It went from 2.39% for the biocomposites in the presence of the dispersing agent to 11.53% for the biocomposites in the absence of BYK W-980, which the microorganisms easily assimilate [31,32]. This was attributed to the reduction of the hydroxyl groups during the fiber pretreatment. The hydrophobicity of the Alfa fibers was reduced when compared to the untreated fibers. The BYK W-980 was easily coated by the PLA matrix, which improved the interfacial bonding that led to less mass loss. In contrast, biocomposites prepared with the dispersing agent BYK W-980 experience fiber distribution and scattering to the point of making their assimilation difficult [33]. In fact, the presence of BYK W-980 at the PLA/Alfa interface inhibits the penetration of water and consequently it causes interference with the action of microorganisms.

In general, the studies encountered in the bibliography are carried out on wood fiber composites and are limited to highlighting microbial development with an evaluation of changes in color or change in mass of the composites. For example, Naumann et al., [34] studied the resistance to Trametes versicolor fungi of PP composites reinforced with 55% by mass of solid beech wood. Growth of fungal mycelium was observed by light microscopy and mass loss was determined after 16 weeks of incubation at 21.5 °C on samples previously dried at 103 °C. The authors estimated a mass loss of 2.2% for composites, whereas it is 45% for solid beech wood.

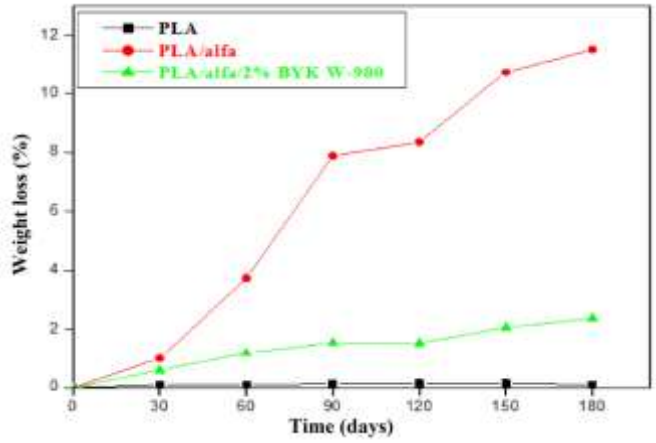

Figure 2: Mass loss rate of PLA, PLA/Alfa biocomposites and PLA/Alfa biocomposites/ 2% BYK W-980 after 180 days of burial in the ground.

The authors observed a surface fungal development following aging but which has no consequences on the chemical and mechanical properties of the composites. Other authors [35] have shown that PVC/wood fiber composites are resistant to Serpula lacrymans, this fungus is responsible for the degradation of half of the buildings constructed of wood in Europe. Thus, they recorded a mass loss after 16 weeks of aging of about 0.8% against a water mass gain of 9.2%, the authors do not specify the incubation conditions.

II. Conclusions

In this work, poly lactic acid reinforced with Alfa fibers with and without the dispersing agent which is BYK W-980 underwent burial in soil aging for duration of 4320 hours (180 days). Considering all the results, we were able to draw the following conclusions:

The study of biodegradation by burial in soil showed that the biodegradability of biocomposites prepared with untreated and treated PLA/Alfa degrade in soil more than those prepared with BYK W-980 for the same burial conditions. Knowing that the PLA buried in the ground is biodegradable after 4 to 5 years, by consecrating in this time interval of burial, we only have the fibers which degrade.

Conflict of interest. The authors report no conflict of interest.

References

[1] F. Torres, S. Rodriguez, A. Saavedra. Green Composite Materials from Biopolymers Reinforced with Agroforestry Waste. Journal of Polymers and the Environment 27, 2651–2673, 2019

[2] R. Siakeng, M. Jawaid, H. Arin, S. Sapuan, M. Asim, N. Saba. Natural fiber reinforced polylactic acid composites: A review. Polymer Composites 40, 446–463, 2018.

[3] M. Asim, K. Abdan, M. Jawaid, M. Nasir, Z. Dashtizadeh, M. Ishak, M.E. Hoque. A review on pineapple leaves fibre and its composites. International Journal of Polymer Science 950567, 2015.

[4] M.H. Gheith, M.A. Aziz, W. Ghori, N. Saba, M. Asim, M. Jawaid. Flexural, thermal and dynamic properties of date palm fibres reinforced epoxy composites. Journal of Materials Research and Technology 8, 853–860, 2019

[5] W. Wang, Q. Han, X. Li, X. Peng, W. Qian. Preparation and characterization of PVC matrix composites with biochemical sludge. Journal of Polymers and the Environment 1-5, 2018

[6] H.N. Dhakal, Z.Y. Zhang, M.O.W. Richardson. Effect of water absorption on the mechanical properties of hemp fibre reinforced unsaturated polyester composites. Composite Science and Technology 67, 1674-1683, 2007

[7] J. Fei, D. Luo, H. Wang, H. Li, J. Huang, W. Luo, X. Duan, X. Effect of nano-SiO2 particles on the carbon fabric/resin friction materials by microwave hydrothermal treatment. Journal of Composite Materials 52(2), 245-252, 2008

[8] J. Hu, M. Guo. Influence of ammonium lignosulfonate on the mechanical and dimensional properties of wood fiber biocomposites reinforced with polylactic acid. Industrial Crops and Products 78, 48-57, 2015

[9] S.K. Hubadillah, M.H.D. Othman, Z. Harun, A.F. Ismail, M.A. Rahman, J. Jaafar. A novel green ceramic hollow fiber membrane (CHFM) derived from rice husk ash as combined adsorbent-separator for efficient heavy metals removal. Ceramics International 43, 4716-4720, 2017

[10] A. Jehdaramarn, S. Pornsuwan, P. Chumsaeng, K. Phomphrai, P. Sangtrirutnugul. Effects of appended hydroxyl groups and ligand chain length on copper coordination and oxidation activity. New Journal of Chemistry 42(1), 654-661, 2018

[11] D. Jhodkar, M. Amarnath, H. Chelladurai, J. Ramkumar, J. Experimental investigations to enhance the machining performance of tungsten carbide tool insert using microwave treatment process. Journal of the Brazilian Society of Mechanical Sciences and Engineering40, 200, 2018

[12] T. Joffre, K. Segerholm, C. Persson, S.L. Bardage, C.L.L. Hendriks, P. Isaksson. Characterization of interfacial stress transfer ability in acetylation-treated wood fibre composites using X-ray microtomography. Industrial Crops and Products 95, 43-49, 2017

[13] R. Jumaidin, S.M. Sapuan, M. Jawaid, M.R. Ishak, J. Sahari. Thermal, mechanical, and physical properties of seaweed/sugar palm fibre reinforced thermoplastic sugar palm starch/agar hybrid composites. International Journal of Biological Macromolecules 97, 606-615, 2017

[14] S.C. Cheison, U. Kulozik. Impact of the environmental conditions and substrate pre-treatment on whey protein hydrolysis: A review. Critical Reviews in Food Science and Nutrition 57, 418-453, 2017

[15] J. Feng, Q. Shi, Y. Chen, X. Huang. Mold Resistance and Water Absorption Of Wood/HDPE And

Bamboo/HDPE Composites. Journal Of Applied Sciences 14, 776–783, 2014

[16] A. Umar, E. Zainudin, S. Sapuan. Effect of accelerated weathering on tensile properties of kenaf reinforced high-density polyethylene composites. Journal of Mechanical Engineering Science 2, 198–205, 2012

[17] M. Bootklad, S. Chantarak, K. Kaewtatip. Novel biocomposites based on wheat gluten and rubber wood sawdust. Journal of Applied Polymer Science doi:10.1002/APP.437052016.

[18] P. Pantyukhov, N. Kolesnikova, A. Popov. Preparation. Polymer Composites: Structure and Properties of Biocomposites Based on Low-Density Polyethylene and Lignocellulosic Fillers. Polymer Composites 37(5), 1461–1472, 2016

[19] H. Ibrahim, D. Hammiche, A. Boukerrou, C. Delaite. Enhancement of Biocomposites Properties Using Different Dispersing Agents. Materials Today: Proceedings 36, 41-46, 2021.

[20] Y. Dong, A. Ghataura, H. Takagi, H.J. Haroosh, A.N. Nakagaito, K.T. Lau. Polylactic acid (PLA) biocomposites reinforced with coir fibres: Evaluation of mechanical performance and multifunctional properties. Composites Part A: Applied Science and Manufacturing 84(6)3, 76–84, 2014

[21] M. Van den Oever, B. Beck, J. Müssig. Agrofibre reinforced poly (lactic acid) composites: Effect of moisture on degradation and mechanical properties. Compos. Part A Appl. Sci. Manuf. 41, 1628–1635, 2010

[22] K. Hamad, M. Kaseem, F. Deri. Rheological and mechanical characterization of poly (lactic acid)/polypropylene polymer blends. Journal of Polymer Research 18, 1799–1806, 2011

[23] Y.F. Shih, C.C. Huang. Polylactic acid (PLA)/banana fiber (BF) biodegradable green composites. Journal of Polymer Research 18, 2335–2340, 2011

[24] A. Satlewal, R. Soni , M. Zaidi, Y. Shouche, R. Goel. Comparative Biodegradation Of HDPE And LDPE Using An Indigenously Developed Microbial Consortium. Journal Of Microbiology And Biotechnology 18,477–482, 2007

[25] C. Scheffert , E.B. Cowling. Natural Resistance Of wood To Microbial Deterioration. Annual Review Of Phytopathology 4, 147–170, 1966

[26] J.M. Schultz. Microstructural Aspects Of Failure In Semicrystalline Polymers. Polymer Engineering and Science 24, 770–785, 1984

[27] W.J. Scott. Water Relations Of Staphylococcus Aureus At 30°C. Australian Journal Of Biological Science 6, 549-564, 1953

[28] T. Dizhbite, G. Telysheva, V. Jurkjane, U. Viesturs. Characterization of the Radical Scavenging Activity Of Lignins-Natural Antioxidants. Bioresource Technology 95, 309–317, 2004

[29] H. Essabir, A. Elkhaoulani, K. Benmoussa, R. Bouhfid, F.Z. Arrakhiz, A. Qaiss. Dynamic Mechanical Thermal Behavior Analysis (Dmta) Of Doum Fibers Reinforced Polypropylene Composites. Materials And Design 51,780–788, 2013

[30] P. Graside, P. Wyeth. Identification Of Cellulosic Fibres by FTIR Spectroscopy. Studies In Conservation 48, 269 275,2003

[31] A. Gregorova, Z. Cibulkova, B. Kosikova, P. Simon. Stabilization Effect of Lignin in Polypropylene and Recycled Polypropylene. Polymer Degradation and Stability 89, 553–558, 2005

[32] J.V. Gulmine, P.R. Janissek, H.M. Heise, L. Akcelrud. Polyethylene Characterization by FTIR. Polymer Testing 21, 557–563, 2002

[33] P.V. Joseph, M.S. Rabello, L.H.C. Mattoso, K. Joseph, S. Thomas. Environmental Effects On The Degradation Behaviour Of Sisal Fibre Reinforced Polypropylene Composites. Composites Science and Technology 62, 1357–1372, 2002

[34] A. Naumann, I. Stephan, M. Noll. Material Resistance of Weathered Wood-Plastic Composites Against Fungal Decay. International Biodeterioration and Biodegradation 75, 28–35, 2012

[35] P. Novak, J. Holan. Estimation Of Weight Decrease f Wood-Polymer Composite Caused By Wood Destroying Fungus Serpula Lacrymans (Wulfen) J. Schröt. Wood Research 58, 173–180, 2013